Noname manuscript No.
(will be inserted by the editor)

Secular Resonances Between Bodies on Close Orbits:
A Case Study of the Himalia Prograde Group of Jovian Irregular Satellites

Daohai Li · **Apostolos A. Christou**

arXiv:1603.05125v1 [astro-ph.EP] 16 Mar 2016

Received: date / Accepted: date

Abstract The gravitational interaction between two objects on similar orbits can effect noticeable changes in the orbital evolution even if the ratio of their masses to that of the central body is vanishingly small. Christou (2005) observed an occasional resonant lock in the differential node $\Delta\Omega$ between two members in the Himalia irregular satellite group of Jupiter in the N-body simulations (corresponding mass ratio $\sim 10^{-9}$). Using a semianalytical approach, we have reproduced this phenomenon. We also demonstrate the existence of two additional types of resonance, involving angle differences $\Delta\omega$ and $\Delta(\Omega+\varpi)$ between two group members. These resonances cause secular oscillations in eccentricity and/or inclination on timescales ~ 1 Myr. We locate these resonances in (a,e,i) space and analyse their topological structure. In subsequent N-body simulations, we confirm these three resonances and find a fourth one involving $\Delta\varpi$. In addition, we study the occurrence rates and the stability of the four resonances from a statistical perspective by integrating 1000 test particles for 100 Myr. We find $\sim 10-30$ librators for each of the resonances. Particularly, the nodal resonance found by Christou is the most stable: 2 particles are observed to stay in libration for the entire integration.

Keywords Irregular Satellites · Secular Resonances · Solar Perturbations · Coorbital Interactions · Nodal resonance · Koza-Lidov mechanism · Kozai cycle

1 Introduction

All planets in the solar system except Mercury and Venus have satellites (see, e.g., Murray and Dermott 1999). Satellites are subject to many types of perturbations, for instance, solar forcing and the oblateness of the host planet.

D. Li
Armagh Observatory, College Hill, Armagh, BT61 9DG, Northern Ireland, UK
School of Mathematics and Physics, Queen's University Belfast, University Road, Belfast, BT7 1NN, Northern Ireland, UK
Tel.: +44 (0)28 3752 2928
Fax: +44 (0)28 3752 7174
E-mail: lidaohai@gmail.com; dli@arm.ac.uk

A. A. Christou
Armagh Observatory, College Hill, Armagh BT61 9DG, Northern Ireland, UK

The Sun's gravity induces a satellite's orbit to precess at a rate, (see, for example, Innanen et al. 1997)

$$\dot{\varpi}_{\odot} \approx \frac{3k^2 m_{\odot}}{4na_{\odot}^3}, \tag{1}$$

where ϖ is the longitude of pericentre of the satellite, k^2 the gravitational constant; $m_{\odot}$ and $a_{\odot}$ are the solar mass and semimajor axis of the Sun's relative motion with respect to the planet; n is the satellite's mean motion and $n = \sqrt{k^2 m/a^3}$ (where m is the mass of the host planet and a the semimajor axis of the satellite). On the other hand, the oblateness of the host planet also causes the orbit to precess at the rate (e.g., Roy 1978)

$$\dot{\varpi}_{J_2} \approx \frac{3}{2} n J_2 \frac{R^2}{a^2}, \tag{2}$$

where J_2 is a measure of the oblateness and R is the equatorial radius of the planet. Equating the two, we find the critical semimajor axis

$$a_{\text{crit}} = \left(\frac{2J_2 R^2 a_{\odot}^3 m}{m_{\odot}} \right)^{1/5}. \tag{3}$$

For a satellite with a below this value, its orbital evolution is mainly controlled by the planetary oblateness, while one with a above this value is governed by solar perturbations. Based on this, Burns (1986) defined irregular satellites as those whose orbital evolution is dominated by the Sun, i.e., with $a > a_{\text{crit}}$ (see also, Goldreich 1966). Thus inherently, this definition mostly places constraints on the average distance from the satellite to the host planet. Apart from the size, their orbits are often highly eccentric and inclined compared to the regular satellites.

The eccentricity and inclination of the irregulars are generally high and their distribution in $[0, 1)$ and $[0^\circ, 180^\circ)$ is not uniform (see, e.g., Jewitt and Haghighipour 2007). For example, the inclinations of them are far from 90°. This feature can be explained by Kozai-Lidov dynamics (Lidov 1962; Kozai 1962) that involves the secular perturbation from the Sun. Under solar forcing, the eccentricity and inclination of the satellite are coupled in such a way that the vertical angular momentum $H \propto \sqrt{1-e^2}\cos i$ is conserved while the eccentricity e and inclination i of the satellite may experience large-amplitude oscillations, especially when i is high. This mechanism causes the absence of satellites with inclinations around 90° (Carruba et al. 2002). We will discuss this effect in detail in Sect. 3.

Most irregular satellites reside on retrograde, rather than prograde, orbits; this relates to the so-called evection phenomenon (Yokoyama et al. 2008; Frouard et al. 2010). Evection is linked to the mean motion of the Sun. If a satellite is too far from the planet, it will be so perturbed by the Sun that its longitude of pericentre ϖ precesses at a rate comparable to the solar mean motion. In this case, the angle $\psi = \varpi - \lambda_{\odot}$ (where $\lambda_{\odot}$ is the mean longitude of Sun) may librate; the angular momentum $G \propto \sqrt{1-e^2}$ may oscillate strongly and the eccentricity may grow from ~ 0 to 0.6 (Frouard et al. 2010). Thus the evection effect places constraints on the stability of irregular satellites and influences their orbital distribution. Furthermore, this effect is not symmetrical with respect to the inclination of 90° because for prograde orbits, $\varpi = \Omega + \omega$ (where Ω is the longitude of the ascending node and ω the argument of pericentre) while for retrograde orbits, ϖ is the difference of the two angles. As a result, the eccentricity of a prograde orbit is excited more efficiently than a retrograde one, providing a possible mechanism to explain why the retrograde regime harbours more irregular satellites (Nesvorný et al. 2003).

A prominent feature of the irregular satellite population is that they form groups or families (Nesvorný et al. 2003; Sheppard and Jewitt 2003). Members of the same family have similar orbital elements. Families are thought to be the products of collisional evolution. Nesvorný et al. (2003) used the Gauss equations to infer the degree of dispersion within different groups of irregular satellites. They found that the Himalia family is more widely dispersed than expected for a group of collisional fragments. Beaugé et al. (2006) and Beaugé and Nesvorný (2007) developed a high order analytical method and used it to calculate accurate precession rates of irregular satellites and to study the dynamical structure of the Kozai resonance. Based on this method, they determined the locations of secular resonances and compared them with the positions of known irregular satellites; also, a new family around Pasiphae was identified. Hinse et al. (2010) applied the MEGNO technique to jovian irregular satellites and identified chaotic and quasi-periodic regions; they also found some high-order mean motion resonances. Using similar methods, Frouard et al. (2011) reported a number of resonances related to the Great Inequality and revealed the chaotic diffusion in different irregular satellite groups.

All of the above work has assumed the irregular satellites to be massless. However, in a manner similar to asteroid families (e.g., Carruba et al. 2003) a massive member of a satellite family could exert strong perturbations on the smaller members and scatter their orbits; Christou (2005) found that, gravitational scattering by Himalia operating over the age of the solar system could be responsible for the large velocity dispersion observed by Nesvorný et al. (2003). Christou used this effect to place constraints on the mass of Himalia. He also observed a transient resonant lock between the nodes of Himalia and Lysithea, another satellite in the family. Thus we suppose a massive member could have significant effects on the orbital evolution of the group and this phenomenon needs further study. Here, as a case study, we focus our attention on the Himalia group of Jupiter and particularly on the resonances identified by Christou.

The paper is organised as follows: in Sect. 2, we introduce the Himalia group, the phenomenon of "nodal libration" and the model used to study it. Then in Sect. 3, we describe our semianalytical approach to model the nodal libration and introduce other resonant phenomena. The results of N-body simulations are presented in Sect. 4. Finally, Sect. 5 is devoted to the conclusions and discussions.

2 The Himalia group, a nodal resonance and our model

The Himalia group is a prograde jovian irregular satellite group with five members: Himalia, Elara, Lysithea, Leda and Dia. Himalia is the largest member that carries the group name; it is at least 8 times more massive than any of the other four known members[1]. Emelyanov (2005) studied the perturbation of Himalia on other satellites and estimated the mass to be $k^2 m = (0.28 \pm 0.04)$ km^3/s^2, consistent with the estimate of Christou (2005) based on its scattering effect. We adopt this mass estimate throughout the paper. The mean semimajor axis, eccentricity and inclination of the group are 0.078 AU, 0.18 and 28°, respectively.

In Christou (2005), where the main purpose was to study the influence of gravitational scattering within the Himalia group, the effects of the Sun, Saturn and jovian oblateness (corrected for the additional mass of Galilean satellites) were considered; Himalia and Elara

[1] Dia was discovered in 2000 and then lost. It was recently recovered by S. S. Sheppard; see http://dtm.carnegiescience.edu/news/long-lost-moon-jupiter-found. For the mass estimates of the members, see http://ssd.jpl.nasa.gov/?sat_phys_par. For orbital elements, see http://ssd.jpl.nasa.gov/?sat_elem. Parameters of other satellites from the latter two links will be used in Sect. 5.

were assumed to be massive and other family members were massless. In such a configuration, it was found that the difference between the longitudes of the nodes of Lysithea and Himalia $\Delta\Omega = \Omega_{\rm L} - \Omega_{\rm H}$ could occasionally librate around π on a timescale of 1 Myr with the amplitude of the oscillation in inclination being $\sim 0.1^\circ$ (see figs. 4 and 5 of that work). Christou also reported that, on entering and leaving the libration, significant changes in the inclination can occur. This provides a fast channel for the evolution of inclination and may contribute to the large relative velocity dispersion in the Himalia group. We refer to this phenomenon as "nodal resonance" or "nodal libration" hereafter.

Here, our goal is to specifically study this dynamical phenomenon. To isolate the relevant dynamics, we work within a restricted four-body problem model containing Jupiter, the Sun, a massive Himalia and a massless test particle; see Fig 1. Here, all bodies revolve around Jupiter (in the relative sense). The Sun is assumed to be on a circular orbit.

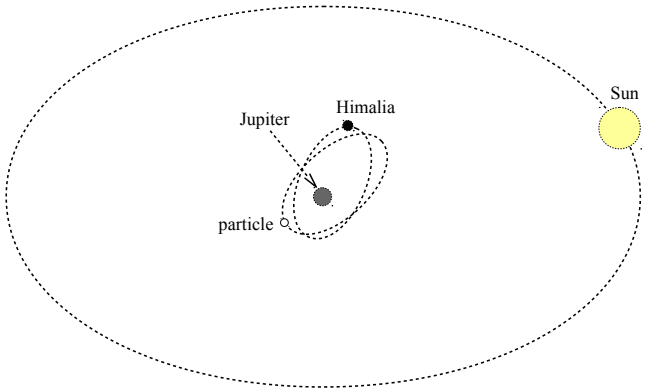

Fig. 1 Illustration of the system that consists of Jupiter, the Sun, Himalia and a particle

In the following sections, we tackle this four-body problem with both semianalytical and fully numerical methods.

3 Semianalytical approach

Our strategy is to split the four-body problem of Jupiter-Sun-Himalia-particle into two restricted three-body problems that can be tackled separately using perturbation analysis. The first includes Jupiter, the Sun and Himalia. Since the mass of Himalia is vanishingly small compared with those of Jupiter and the Sun, it is assumed to be also massless in this part. Thus Himalia and the particle can be studied using the same technique. The second three-body problem is comprised of Jupiter, massive Himalia and the massless particle. We describe in detail the methods dealing with the two restricted three-body problems in the following subsections. Then we explain how we combine the two.

In this paper, we use a normalised unit system in which the Solar mass is 1; jovian semi-major axis is 1; gravitational constant is 1; thus the orbital period of Jupiter is approximately 2π; in practice, we have used 2π in time conversion for the N-body simulations described in Sect. 4.

3.1 Kozai dynamics in the Jupiter-Sun-satellite restricted three-body problem

In the first instance, solar perturbations dominate the evolution of Himalia and the particle. A substantial body of literature has dealt with such "hierarchical" planet-Sun-satellite problems and has discussed the Kozai-Lidov mechanism (Lidov 1962; Kozai 1962). There, the Hamiltonian of the system is expanded in terms of the ratio of semimajor axis of the satellite to that of the Sun (we denote this ratio as $\alpha = a/a_\odot$ hereafter) and only the leading order terms (of order α^2; the "quadrupole" Hamiltonian) are retained. Actually, in our simple model, the Sun has zero eccentricity, causing the octupole Hamiltonian (of order α^3) to be zero (see, e.g., Krymolowski and Mazeh 1999; Naoz et al. 2013). Then the mean anomalies of the Sun and Himalia are eliminated. Owing to a "happy coincidence" (Lidov and Ziglin 1976), the quadrupole secular Hamiltonian is integrable. Specifically, this Hamiltonian is

$$F = \frac{k^2 m_\odot a^2}{16 a_\odot^3}\left[\left(-15e^2\cos(2\omega)+9e^2+6\right)\cos^2 i + 15e^2\cos(2\omega) - 3e^2 - 2\right], \qquad (4)$$

in which k^2 is the gravitational constant and $m_\odot$ the mass of the Sun; a and $a_\odot$ are semimajor axes of the satellite and the Sun; e, i and ω are the satellite's orbital eccentricity, inclination and argument of pericentre, respectively (Kozai 1962; Naoz et al. 2013); this Hamiltonian and its simplified forms will be referred to as the "Kozai Hamiltonian" hereafter. Apparently, the Hamiltonian F and semimajor axis a are conserved. As the longitude of the ascending node Ω does not appear in Eq. (4), the vertical component of the angular momentum $H \propto \sqrt{1-e^2}\cos i$ is constant as well. For a dynamical system governed by this Hamiltonian, ω may librate around $\pm\pi/2$ while the angular momentum $G \propto \sqrt{1-e^2}$ may experience large amplitude oscillation, giving rise to the Kozai resonance. All four giant planets have such satellites (Nicholson et al. 2008). The libration in ω requires the inclination to exceed $\approx 40^\circ$; this is not the situation for the Himalia group. Generally, such evolution under solar perturbation is referred to as a "Kozai cycle". In Kozai theory, the reference plane is the orbital plane of Jupiter; this frame is used throughout the paper.

With this Hamiltonian, we can obtain the expressions for the nodal and apsidal precession rates of the satellite. The Hamiltonian will be further simplified in Subsect. 3.3.

3.2 Satellite interaction in the Jupiter-Himalia-particle restricted three-body problem

Here, we consider the subsystem comprised of Jupiter, Himalia and a massless test particle.

Since the orbits of the two satellites are close and may cross, the traditional expansion of the disturbing function (e.g., Murray and Dermott 1999) is not applicable here. To tackle this, we resort to treating the problem under the framework of coorbital theory. The crucial differences between coorbital theory and the conventional treatment lie in the expansion in the disturbing function and in the elimination of the mean anomalies. In coorbital theory, no expansion is made with respect to the ratio of semimajor axes. The mean anomalies of the two orbits are eliminated in a combined manner so that the difference in the mean longitudes $\Delta\lambda$ remains. This enables the study of the variation of the relative semimajor axis Δa (see, for example, Message 1966; Morais 1999). When studying the secular evolution of the system, $\Delta\lambda$ is eliminated.

We follow Hénon and Petit (1986) (see also, Namouni 1999) and use the relative quantities, e.g., the relative vector eccentricity $\mathbf{e}_\mathrm{r} = \mathbf{e}_\mathrm{P} - \mathbf{e}_\mathrm{H} = (e_\mathrm{P}\cos\varpi_\mathrm{P} - e_\mathrm{H}\cos\varpi_\mathrm{H}, e_\mathrm{P}\sin\varpi_\mathrm{P} - e_\mathrm{H}\sin\varpi_\mathrm{H})$ (where ϖ is the longitude of pericentre) of the particle relative to Himalia.

We assume that Himalia and the particle are on similar orbits (i.e., with similar semimajor axes, eccentricities and inclinations), that their eccentricities and inclinations are much smaller than unity and that their total mass is far smaller than that of the central body, Jupiter. The semimajor axes, eccentricities and inclinations of the members of the group are restricted to small ranges and the eccentricities are relatively small, satisfying the requirement of coorbital theory. However, the inclination of the Himalia group is about 0.5 rad. As the main purpose of this section is to describe the dynamical structure qualitatively but not to provide a precise quantitative description of the orbital evolution, we divide all inclinations by a factor of 3 in this section wherever coorbital theory is involved. In this way, the eccentricities and inclinations are all around 0.17, better suiting the expansion described below. We will briefly discuss what the situation is if we apply the original inclinations in Sect. 5. In this setting, the motion of the two satellites can be expressed in a frame whose origin revolves around Jupiter on a circular orbit of semimajor axis a_0 ($a_0 \in (\min(a_\mathrm{H}, a_\mathrm{P}), \max(a_\mathrm{H}, a_\mathrm{P}))$); the frame also rotates along its z-axis at an angular velocity of $n_0 = \sqrt{k^2(m_\mathrm{J}+m_\mathrm{H})/a_0^3}$ (where m_J and m_H are masses of Jupiter and Himalia, respectively; the particle is massless). Omitting higher order terms in e and i and assuming that the two satellites are not generally interacting, the Cartesian coordinates of Himalia in this rotating frame can be expressed as the following functions of time (Hénon and Petit 1986; Namouni 1999)

$$\begin{cases} x_\mathrm{H} = a_\mathrm{H}(h_\mathrm{H}\cos n_0 t + k_\mathrm{H}\sin n_0 t) + (a_\mathrm{H} - a_0) \\ y_\mathrm{H} = -2a_\mathrm{H}(h_\mathrm{H}\sin n_0 t - k_\mathrm{H}\cos n_0 t) - \dfrac{3}{2}(a_\mathrm{H} - a_0)(n_0 t - \lambda_\mathrm{H}) \\ z_\mathrm{H} = a_\mathrm{H}(p_\mathrm{H}\cos n_0 t + q_\mathrm{H}\sin n_0 t)\,, \end{cases} \tag{5}$$

where a_H, $h_\mathrm{H} = e_\mathrm{H}\cos\varpi_\mathrm{H}$, $k_\mathrm{H} = e_\mathrm{H}\sin\varpi_\mathrm{H}$, $p_\mathrm{H} = i_\mathrm{H}\cos\Omega_\mathrm{H}$, $q_\mathrm{H} = i_\mathrm{H}\sin\Omega_\mathrm{H}$ and λ_H are the regular orbital elements of Himalia; similar equations apply for the particle. From the linearity of these expressions, it can be seen that analogous expressions exist for the motion of the particle relative to Himalia and the relative e and i are constant.

On account of a massive Himalia, the relative eccentricity and inclination begin to evolve. It has been shown the secular evolution of relative e and i observe the following potential (Luciani et al. 1995; Namouni 1999)

$$R = \frac{k^2\mu(m_\mathrm{J}+m_\mathrm{H})}{2\pi a_0}\log\Delta\,, \tag{6}$$

where when $e_\mathrm{r}|\cos\omega_\mathrm{r}| \geq |a_\mathrm{r}|$,

$$\Delta = 2e_\mathrm{r}i_\mathrm{r}|\cos\omega_\mathrm{r}| + i_\mathrm{r}^2 + e_\mathrm{r}^2\,, \tag{7}$$

and when $e_\mathrm{r}|\cos\omega_\mathrm{r}| < |a_\mathrm{r}|$,

$$\begin{aligned} \Delta = \sqrt{2}|a_\mathrm{r}|\sqrt{\sqrt{4e_\mathrm{r}^2 i_\mathrm{r}^2\sin^2\omega_\mathrm{r} + (-i_\mathrm{r}^2 + e_\mathrm{r}^2 - a_\mathrm{r}^2)^2} + i_\mathrm{r}^2 - e_\mathrm{r}^2 + a_\mathrm{r}^2} \\ + \sqrt{4e_\mathrm{r}^2 i_\mathrm{r}^2\sin^2\omega_\mathrm{r} + (-i_\mathrm{r}^2 + e_\mathrm{r}^2 - a_\mathrm{r}^2)^2} + a_\mathrm{r}^2\,. \end{aligned} \tag{8}$$

In the above expressions, $\mu = m_\mathrm{H}/m_\mathrm{J}$, $a_\mathrm{r} = (a_\mathrm{P} - a_\mathrm{H})/a_0$, $e_\mathrm{r} = \sqrt{h_\mathrm{r}^2 + k_\mathrm{r}^2}$, $i_\mathrm{r} = \sqrt{p_\mathrm{r}^2 + q_r^2}$, $\varpi_\mathrm{r} = \tan^{-1}(k_\mathrm{r}/h_\mathrm{r})$, $\Omega_\mathrm{r} = \tan^{-1}(q_\mathrm{r}/p_\mathrm{r})$, $\omega_\mathrm{r} = \varpi_\mathrm{r} - \Omega_\mathrm{r}$, $h_\mathrm{r} = h_\mathrm{P} - h_\mathrm{H}$, $k_\mathrm{r} = k_\mathrm{P} - k_\mathrm{H}$, $p_\mathrm{r} =$

$p_{\rm P}-p_{\rm H}$ and $q_{\rm r}=q_{\rm P}-q_{\rm H}$ (the relative elements). The equations of motion are then (Namouni 1999)

$$\begin{aligned} \dot{h}_{\rm r} &= \frac{1}{n_0}\frac{\partial R}{\partial k_{\rm r}}, \qquad & \dot{k}_{\rm r} &= -\frac{1}{n_0}\frac{\partial R}{\partial h_{\rm r}}, \\ \dot{p}_{\rm r} &= \frac{1}{n_0}\frac{\partial R}{\partial q_{\rm r}}, \qquad & \dot{q}_{\rm r} &= -\frac{1}{n_0}\frac{\partial R}{\partial p_{\rm r}}. \end{aligned} \tag{9}$$

The coorbital secular potential (6) causes variations in e_r and i_r; it also gives rise to precession in ϖ_r and Ω_r (Namouni 1999). These effects, in turn, are reflected in the evolution of the particle's elements $(\varpi_{\rm P}, e_{\rm P})$ and $(\Omega_{\rm P}, i_{\rm P})$.

3.3 Secular dynamics of the Jupiter-Sun-Himalia-particle system

Having isolated the relevant dynamics in the two sub-problems discussed in Subsects. 3.1 and 3.2, we now want to combine them. This is done so that both Himalia and the test particle experience solar perturbation through the Kozai Hamiltonian (4); to this we add the gravitational influence on the particle from Himalia by applying (9) to potential (6) and adding the corresponding variation rates to the particle. Thus the equations of motion are

$$\dot{\sigma}_{\rm H} = f^{\odot}(\sigma_{\rm H}) \quad \text{and} \quad \dot{\sigma}_{\rm P} = f^{\odot}(\sigma_{\rm P}) + f^{\rm coorb}(\sigma_{\rm r}), \tag{10}$$

where σ is an arbitrary orbital element; $f^{\odot}$ refers to the solar perturbation and is a function of the elements of Himalia or the particle; $f^{\rm coorb}$ represents the contribution from the coorbital interaction potential and is a function of the relative elements. We now have an eight-dimensional system of $(\varpi_{\rm H}, e_{\rm H}; \varpi_{\rm P}, e_{\rm P}; \Omega_{\rm H}, i_{\rm H}; \Omega_{\rm P}, i_{\rm P})$.

The evolution of the particle is generally dominated by solar perturbations even when perturbations by both the Sun and Himalia are considered. We use a simple example to demonstrate this point. According to Eqs. (4) and (6), and for the nominal orbits of Himalia and Lysithea (as the particle), the timescales of precession in $\varpi_{\rm P}$ and $\Omega_{\rm P}$ induced by the coorbital potential are $\tau_{\varpi}^{\rm coorb} \sim 2\pi/\dot{\varpi}^{\rm coorb} \approx 2.7\times10^7$ and $\tau_{\Omega}^{\rm coorb} \sim 2\pi/\dot{\Omega}^{\rm coorb} \approx 2.8\times10^7$. For solar perturbations, the corresponding timescales are $\tau_{\varpi}^{\odot} \sim 2\pi/\dot{\varpi}^{\odot} \approx 1.5\times10^2$ and $\tau_{\Omega}^{\odot} \sim 2\pi/\dot{\Omega}^{\odot} \approx 1.4\times10^2$. Noting that, according to Christou (2005), the timescale of nodal libration is $\sim 10^6$, thus the effects of a Kozai cycle should be considered as "fast" and can be eliminated when tackling nodal libration.

Assuming that within a Kozai cycle, changes in eccentricity is small ($\Delta e \ll 1$) and applying some algebraic manipulations (see Appendix A for details), we have the following "averaged" Kozai Hamiltonian

$$F_{\rm K} = -\frac{k^2 m_{\odot} a^2}{16 a_{\odot}^3}\left(2+3e^2\right)\left(1-3\cos^2 i\right), \tag{11}$$

where e and i are the "averaged" quantities over a Kozai cycle compared to the original ones in Eq. (4). With this Hamiltonian, the precession rates of Ω and ϖ are constant. Rates of group members are close with similar a, e and i.

As shown above, the influence of Himalia is several orders of magnitude smaller than that of the Sun. We suggest that, the libration in $\Delta\Omega$ is only possible where $\mathrm{d}\Delta\Omega/\mathrm{d}t$ is vanishingly small under solar perturbations. With the Hamiltonian (11), we define a surface in (a,e,i) space where all points on it share the same nodal precession rate with Himalia: $\dot{\Omega}(a,e,i) = \dot{\Omega}|_{\rm H}$ (since $\dot{\Omega}$ is a function depending only on a, e and i); we call this a Surface

of Equal Precession Rate (SEPR) in Ω. We show the SEPR in Fig. 2; it is conceptually similar to those discussed in Williams and Faulkner (1981) in the contact of secular resonances in the main asteroid belt. Note that, until now, we do not assume small eccentricity or inclination for the Kozai Hamiltonian; thus the SEPR applies to the real Himalia group, whose inclination is about 0.5 rad.

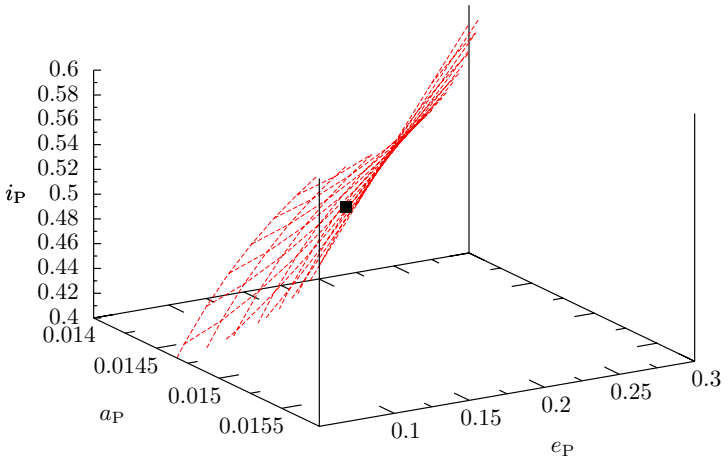

Fig. 2 The surface of equal precession rate in Ω in (a,e,i) space. The location of the surface is calculated using the Kozai Hamiltonian (11) without expansion in eccentricity or inclination. Points on the surface share the same precession rate as Himalia in Ω. The black square represents the location of Himalia

However, as the coorbital potential (6) results from an expansion in eccentricity and inclination, combining it with the full expression for the Kozai potential (11) seems superfluous. Hence, we also expand (11) in e and i, retaining terms up to order four to arrive at the following Kozai Hamiltonian

$$F = -\frac{k^2 m_\odot a^2}{16 a_\odot^3}\left(2i^4 - 9e^2 i^2 - 6i^2 + 6e^2\right). \tag{12}$$

We then rewrite the Hamiltonian in normalised Poincaré conjugate variables, and again we adopt expansions in e and i. The variables are

$$\bar{g} = -\varpi = -(\Omega + \omega), \bar{G} = e^2/2; \quad \bar{h} = -\Omega, \bar{H} = i^2/2. \tag{13}$$

Under the new variable set, the Kozai Hamiltonian becomes

$$F = -\frac{k m_\odot a^{3/2}}{4\sqrt{m_\jmath}\, a_\odot^{\,3}}\left(2\bar{H}^2 - 9\bar{G}\bar{H} - 3\bar{H} + 3\bar{G}\right). \tag{14}$$

Since now the variables are the normalised angular momenta, we introduce a factor of $k\sqrt{m_\jmath a}$ into the coefficient of (14) to preserve the Hamiltonian property. To better separate

"slow" and "fast" angles, we apply the following canonical transformation:

$$\begin{aligned} \bar{g}_\mathrm{f} &= \bar{g}_\mathrm{P}, & \bar{G}_\mathrm{f} &= \bar{G}_\mathrm{P} + \bar{G}_\mathrm{H}; \\ \bar{g}_\mathrm{s} &= \bar{g}_\mathrm{P} - \bar{g}_\mathrm{H}, & \bar{G}_\mathrm{s} &= -\bar{G}_\mathrm{H}; \\ \bar{h}_\mathrm{f} &= \bar{h}_\mathrm{P}, & \bar{H}_\mathrm{f} &= \bar{H}_\mathrm{P} + \bar{H}_\mathrm{H}; \\ \bar{h}_\mathrm{s} &= \bar{h}_\mathrm{P} - \bar{h}_\mathrm{H}, & \bar{H}_\mathrm{s} &= -\bar{H}_\mathrm{H}. \end{aligned} \tag{15}$$

On the right-hand side of the above expressions, $(\bar{g}, \bar{G})$ and $(\bar{h}, \bar{H})$ are conjugate normalised Poincaré variables with subscripts "H" and "P" referring to Himalia and the particle, respectively. On the left-hand side, angles (represented with lower-cased letters) with subscript "f" are faster compared to those with subscript "s", since the former are differences between, while the latter are identical to, the original angles; the conjugate momenta are represented with capital letters.

Thus the Kozai Hamiltonian of both Himalia and the particle assumes the following form

$$\begin{aligned} F_\mathrm{S} = C_\mathrm{P} \big(& 2\bar{H}_\mathrm{s}^2 + 4\bar{H}_\mathrm{f}\bar{H}_\mathrm{s} - 9\bar{G}_\mathrm{s}\bar{H}_\mathrm{s} - 9\bar{G}_\mathrm{f}\bar{H}_\mathrm{s} - 3\bar{H}_\mathrm{s} + 2\bar{H}_\mathrm{f}^2 \\ & - 9\bar{G}_\mathrm{s}\bar{H}_\mathrm{f} - 9\bar{G}_\mathrm{f}\bar{H}_\mathrm{f} - 3\bar{H}_\mathrm{f} + 3\bar{G}_\mathrm{s} + 3\bar{G}_\mathrm{f} \big) \\ + C_\mathrm{H} \big(& 2\bar{H}_\mathrm{s}^2 - 9\bar{G}_\mathrm{s}\bar{H}_\mathrm{s} + 3\bar{H}_\mathrm{s} - 3\bar{G}_\mathrm{s} \big) \,, \end{aligned} \tag{16}$$

with coefficients $C_\mathrm{P} = -km_\odot a_\mathrm{P}^{3/2}/(4m_\mathrm{J}^{1/2}a_\odot{}^3)$ and $C_\mathrm{H} = -km_\odot a_\mathrm{H}^{3/2}/(4m_\mathrm{J}^{1/2}a_\odot{}^3)$, where a_H and a_P are the semimajor axes of Himalia and the test particle, respectively.

The coorbital potential (6) is a branch function. Note that within the satellite group, the quantity $a_\mathrm{r} = (a_\mathrm{P} - a_\mathrm{H})/a_0$ is always small. Taking the orbital elements of Lysithea for example, $a_\mathrm{r} \approx 0.02$ while e_r is of order 10^{-1}. Thus the condition $e_\mathrm{r}|\cos\omega_\mathrm{r}| < a_\mathrm{r}$ is rarely satisfied and the potential form (7) dominates. We omit the other form and presume that the potential only takes this form.

Again, we emphasise that, what matters is the difference between the nodes of the particle and Himalia. Hence, any effects that operate on timescales comparable to $2\pi/\dot{\Omega}$ are considered "fast" (cf. transformation (15)) and we need to eliminate them. Since we have assumed constant eccentricity and inclination in the Kozai theory (11) and (14), there is nothing to remove in the Kozai Hamiltonian. However, the short timescale effects in the coorbital potential (6) need elimination. We proceed as follows. First, we substitute the variables in the coorbital potential to express it in the same variables as the Kozai Hamiltonian (16). Noting that the fast angles are controlled primarily by the Kozai potential, they precess evenly with time (cf. Eq. (16)). Hence we perform two finite integrations and arrive at the "slow" coorbital potential[2]:

$$\begin{aligned} R_\mathrm{S} =& \frac{1}{4\pi^2}\int_0^{2\pi} \mathrm{d}\bar{g}_\mathrm{f} \int_0^{2\pi} R(\bar{g}_\mathrm{f}, \bar{G}_\mathrm{f}; \bar{h}_\mathrm{f}, \bar{H}_\mathrm{f}; \bar{g}_\mathrm{s}, \bar{G}_\mathrm{s}; \bar{h}_\mathrm{s}, \bar{H}_\mathrm{s})\, \mathrm{d}\bar{h}_\mathrm{f} \\ =& \frac{\mu n_0}{\pi^2} \left\{ \Im \left[\mathrm{Li}_2\left(\frac{\mathrm{i}i_\mathrm{r}}{e_\mathrm{r}}\right) - \mathrm{Li}_2\left(-\frac{\mathrm{i}i_\mathrm{r}}{e_\mathrm{r}}\right) \right] + \log e_\mathrm{r} \right\}. \end{aligned} \tag{17}$$

Here, the variables have the same meaning as in Eqs. (6) and (7); i is the unit imaginary number; $\Im$ represents the imaginary part; Li is the polylogarithm function defined as (e.g., Weisstein 1999)

$$\mathrm{Li}_n(z) = \sum_{k=1}^{\infty} \frac{z^k}{k^n} \tag{18}$$

[2] Though the form appears asymmetric in e_r and i_r, exchanging e_r and i_r will not alter the value.

where z is a complex number and $|z| < 1$.

We have now reached a system devoid of "fast" effects, i.e., those operating on timescales similar to a Kozai cycle. Note that the coorbital potential is *not* a Hamiltonian in these variables (we show this in the Appendix B). However, we can still write down the equations of motion of the system as

$$\begin{aligned} \dot{\bar{g}}_{\rm s} &= f^{\odot}_{\rm s,g} + f^{\rm coorb}_{\rm s,g}, \quad \dot{\bar{G}}_{\rm f} = f^{\rm coorb}_{\rm f,G}; \\ \dot{\bar{h}}_{\rm s} &= f^{\odot}_{\rm s,h} + f^{\rm coorb}_{\rm s,h}, \quad \dot{\bar{H}}_{\rm f} = f^{\rm coorb}_{\rm f,H}. \end{aligned} \tag{19}$$

Here $f^{\odot}_{\rm s,g}$ is the rate of solar-driven variation in $\bar{g}_{\rm s}$ and is derived directly from partial differentiation of the Kozai Hamiltonian (16). The derivation of the coorbital potential contribution $f^{\rm coorb}_{\rm f,G}$ and $f^{\rm coorb}_{\rm s,g}$ is not so straightforward. Using the potential (17) and the equations of motion (9), we can express the variational rates of the relative variables $h_{\rm r}$ and $k_{\rm r}$ exerted by Himalia. The rates of the orbital elements of the particle are related to these rates through Eq. (10). Then the transformation (15) allows us to derive the rates $f^{\rm coorb}_{\rm f,G}$ and $f^{\rm coorb}_{\rm s,g}$ in Eq. (19). Analogous relations exist for $\bar{h}_{\rm f}$ and $\bar{H}_{\rm s}$. In this way, we arrive at the above equations of motion (19). In essence, what we have is a four-dimensional system of $(\bar{g}_{\rm s}; \bar{G}_{\rm f}; \bar{h}_{\rm s}; \bar{H}_{\rm f})$.

When describing the dynamics of the system, we still use the original orbital elements $\Delta\Omega = \Omega_{\rm P} - \Omega_{\rm H}$, $\Delta\varpi = \varpi_{\rm P} - \varpi_{\rm H}$, $e_{\rm P}$ and $i_{\rm P}$.

3.4 General dynamics

With the equations of motion above, we are able to integrate the system (19) numerically to investigate its evolution[3]. We run test integrations and find that, at most locations in phase space, the angles $\Delta\Omega$ and $\Delta\varpi$ circulate with small amplitude oscillations in $e_{\rm P}$ and $i_{\rm P}$. This is not unexpected and results from the fact that, for positions in the (a, e, i) space far from the SEPR, solar perturbations cause $\Delta\Omega$ and $\Delta\varpi$ to circulate fast, while the coorbital potential contributes minor changes to the precession rates and introduces small amplitude variations in $e_{\rm P}$ and $i_{\rm P}$.

However, when near the SEPR, Himalia can be as efficient as the Sun in changing the orbital evolution; we show this in the following subsections.

3.5 Nodal resonance

In Fig. 3, we show an example of nodal libration in $\Delta\Omega$ in our integrations of Eq. (19). As observed in Christou (2005), the angle $\Delta\Omega$ librates around π. While the inclination oscillates in concert with the libration in the nodal difference, the eccentricity undergoes only small amplitude and short time-scale variations. In fact, the eccentricity is a quasi-conserved quantity here and in the two-dimensional system in Subsect. 3.7, it is actually constant. The timescale of nodal libration is of order 10^6 ($\sim$ 1 Myr) and the changes in inclination are of order 10^{-3}. To prove the postulate that the librator oscillates around the SEPR when in resonance, we plot the signed distance from the particle to the surface in the same figure. From the plot, it is clear that, when above the SEPR, $\Delta\Omega$ increases and vice

[3] All integrations of the equations of motion derived from Kozai and/or coorbital theory are carried out with a 7th order Runge-Kutta method; the step-size is adjusted with an 8th order error estimate. The single step error tolerance is 10^{-14}.

versa[4]. Inherently, when in nodal libration, the particle is restricted to be near the surface and to cross it regularly. This also shows the dominance of the Sun.

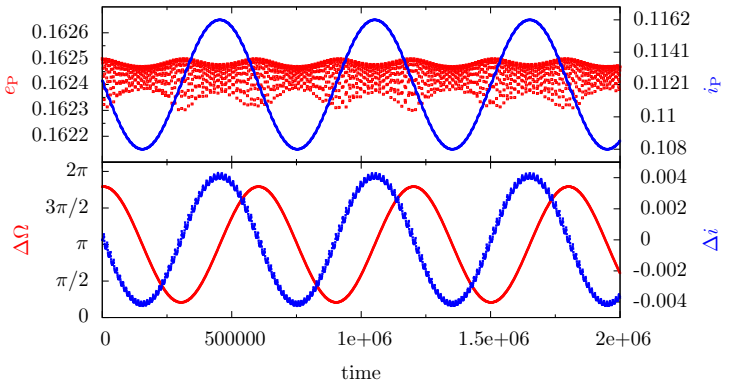

Fig. 3 An example of nodal libration from the four-dimensional system (19). Top panel: e (red) and i (blue); bottom panel: $\Delta\Omega$ (red) and the signed "distance" to the SEPR (blue); x-axis: time in our adopted unit. Since what matters is not the absolute "distance" but the relative position of the librating particle with respect to the SEPR, we use the quantity Δi to represent this relation. Δi is the distance from the particle to the point in the SEPR with the same a and e. Thus $\Delta i > 0$ means the test particle is above the SEPR and vice versa

3.6 Three additional slow angles

Using the same method in Subsect. 3.3, we find that the SEPR in terms of the pericentre $\dot{\varpi}(a,e,i) = \dot{\varpi}|_{\rm H}$ exists. Furthermore, the SEPRs corresponding to the angle combinations $\frac{{\rm d}(\varpi-\Omega)}{{\rm d}t}(a,e,i) = \frac{{\rm d}\omega}{{\rm d}t}(a,e,i) = \frac{{\rm d}\omega}{{\rm d}t}|_{\rm H}$ and $\frac{{\rm d}(\Omega+\varpi)}{{\rm d}t}(a,e,i) = \frac{{\rm d}(\Omega+\varpi)}{{\rm d}t}|_{\rm H}$ can be readily computed. We present them together with the SEPR in Ω in Fig. 4. The four surfaces share the same intersection curve.

Using our semianalytical model, we find that two of these three angles, $\Delta\omega = \Delta(\varpi - \Omega) = \omega_{\rm P} - \omega_{\rm H}$ and $\Delta(\Omega+\varpi) = (\Omega_{\rm P}+\varpi_{\rm P}) - (\Omega_{\rm H}+\varpi_{\rm H})$, can librate. We show examples of these resonances in Figs. 5 and 6. Interestingly, we do not find libration in the angle $\Delta\varpi = \varpi_{\rm P} - \varpi_{\rm H}$; instead there is only slow circulation near its SEPR; see Fig. 7.

In the case of the $\Delta\omega$ resonance in Fig. 5, while the angle librates about π, the variations of eccentricity and inclination are anti-correlated. This behaviour is reminiscent of the Kozai resonance (Kozai 1962). As we will show in the next subsection, the quasi-conserved quantity is $(e_{\rm P}^2 + i_{\rm P}^2)/2$, the component of the angular momentum along the z-axis; we plot this quantity in the same figure.

For the resonance of $\Delta(\Omega+\varpi)$ in Fig. 6, the angle librates about 0 while the eccentricity and inclination are correlated. The quasi-conserved quantity in this case is $(e_{\rm P}^2 - i_{\rm P}^2)/2$.

What we have shown here are the examples where the angles librate. When outside libration but still close to the SEPRs, the angles circulate slowly and monotonically increase

[4] In fact, the node precesses with negative rates. Thus when above the SEPR, the test particle has smaller absolute precession rate.

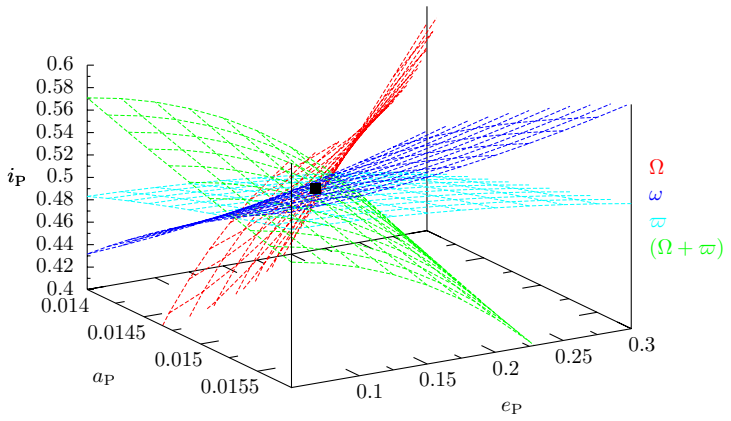

Fig. 4 The surfaces of equal precession rate in Ω, $\omega = (\varpi - \Omega)$, ϖ and $(\Omega + \varpi)$ in (a, e, i) space. They are evaluated in the same way as Fig. 2; the layout of the three axes and the viewing angle are also the same. Particles on these surfaces share the same precession rates in the angles Ω (red), $\omega = (\varpi - \Omega)$ (blue), ϖ (cyan) and $(\Omega + \varpi)$ (green) with Himalia, respectively. The black square marks the position of Himalia. We deliberately choose this viewing angle so that, the normals to the surfaces appear perpendicular to the line of sight

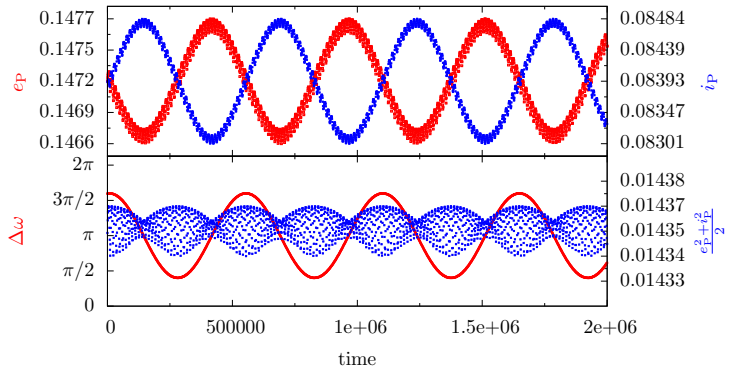

Fig. 5 An illustration of the resonance in the angle $\Delta\omega = \Delta(\varpi - \Omega)$. Top panel: e (red) and i (blue); bottom panel: $\Delta\omega$ (red) and the quasi-conserved quantity $(e_P^2 + i_P^2)/2$ (blue); x-axis: time. This type of resonance is similar to the Kozai resonance

or decrease (since no crossing of the SEPR takes place now) with the actions evolving on the same timescale and in concert, like the case of the angle $\Delta\varpi$ described below.

For particles near the SEPR in ϖ, we detect no libration[5] thus we show an example of slow circulation in Fig. 7. When $\Delta\varpi$ circulates slowly, the eccentricity varies on the same timescale while the inclination experiences only short-period oscillations. In essence, inclination is the quasi-conserved quantity here. In this situation, the test particle cannot cross the SEPR in ϖ, as is shown in the same figure. However, though the distance from

[5] We generate 500 randomly distributed particles on the SEPR in ϖ and integrate them for 2×10^6. Visual check shows no apsidal resonance.

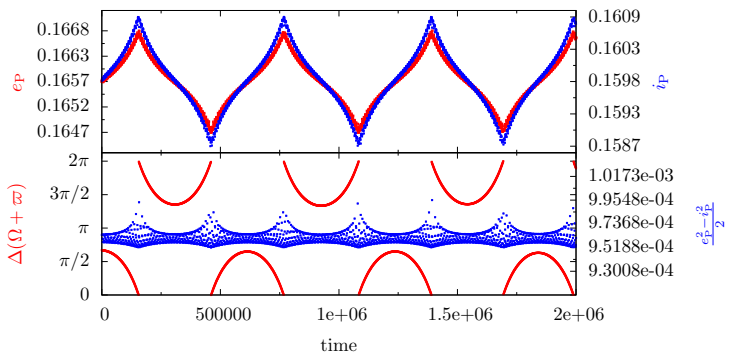

Fig. 6 A representative of the libration in $\Delta(\Omega+\varpi)$. Top panel: e (red) and i (blue); bottom panel: $\Delta(\Omega+\varpi)$ (red) and the quasi-conserved quantity $(e_P^2-i_P^2)/2$ (blue); x-axis: time

the particle to the SEPR remains positive for most of the time, it does become negative for some time. According to the previous reasoning, the distance should not change its sign when in circulation. We suggest that, because of the coorbital potential, the SEPR from Kozai theory does not coincide with the SEPR of the full problem. As will be shown, the coorbital potential causes a small displacement in the surface. Thus although the distance in terms of the SEPR in Kozai potential changes the sign, the distance with respect to the SEPR controlled by both Kozai and coorbital potential does not. See Fig. 9 for the influence of coorbital potential on the equilibrium points (i.e., the real SEPR). In Sect. 5 we discuss the reason why no examples of libration in $\Delta\varpi$ are observed here.

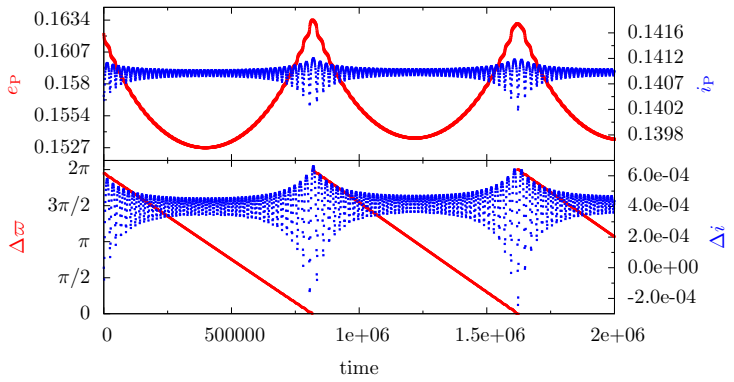

Fig. 7 Typical evolution of the slow circulation of the angle $\Delta\varpi$. Top panel: e (red) and i (blue); bottom panel: $\Delta\varpi$ (red) and the signed "distance" to the SEPR in ϖ (blue); x-axis: time

3.7 Phase space properties for the three types of resonance

Having established that the three types of resonance exist in the four-dimensional system (19), we can reduce the system to two dimensions specifically to study the structure of individual resonances when the frequencies are well separated. We elaborate our approach for the nodal resonance and omit the details for the other two cases. Near the SEPR in Ω and far from the common intersection curve of the four SEPRs, we have $\mathrm{d}\Delta\Omega/\mathrm{d}t \ll \mathrm{d}\Delta\varpi/\mathrm{d}t$. At these positions, the effect of the Sun in altering $\Delta\varpi$ far outweighs that of the coorbital interaction. Thus the evolution in $\Delta\varpi, e_\mathrm{P}$ is dominated by the Sun. In addition, under solar forcing (16), there is only (rapid) precession in $\Delta\varpi$ and no evolution in e. Hence, $\Delta\varpi$ is now a "fast" angle (compared to $\Delta\Omega$) and e_P is constant. To isolate the evolution in $(\Delta\Omega, i_\mathrm{P})$, we can perform the following averaging

$$< \dot{\bar{h}}_\mathrm{s} >= f^{\odot}_{\mathrm{s,h}} + \frac{1}{2\pi}\int_0^{2\pi} f^{\mathrm{coorb}}_{\mathrm{s,h}}\,\mathrm{d}\bar{g}_\mathrm{s}\,, \quad < \dot{\bar{H}}_\mathrm{f} >= \frac{1}{2\pi}\int_0^{2\pi} f^{\mathrm{coorb}}_{\mathrm{f,H}}\,\mathrm{d}\bar{g}_\mathrm{s} \tag{20}$$

to arrive at a two-dimensional system of $(\bar{h}_\mathrm{s}; \bar{H}_\mathrm{f})$ (Cf. Eq. (19)). Here, all effects operating on timescales shorter than that of nodal libration are removed. We plot the evolution in $(\Delta\Omega, i_\mathrm{P})$ space in Fig. 8; we elect to show the inclination relative to an empirically-determined value of 0.22 to highlight the amplitude of the variation. The topological structure of the resonance is clear: the system has two equilibrium points – a stable one with $\Delta\Omega = \pi$ and an unstable one with $\Delta\Omega = 0$; libration around the stable equilibrium point is allowed (which is the resonance we see). Hence, we suggest that with the coorbital potential, each point in the SEPR in Kozai potential is split into the two equilibrium points. This can be shown by setting the variation rates in (20) to be zero. In Fig. 9, we show the positions of the two stationary points as functions of varying e_P. The shift of the equilibrium points from the SEPR indicates the influence of the coorbital potential and is of order 10^{-5}, reflecting the weakness of the coorbital interaction compared to the Kozai dynamics.

Using similar techniques, we generate analogous plots for the resonances involving the angles $\Delta\omega = \Delta(\varpi - \Omega)$ and $\Delta(\Omega + \varpi)$ in Figs. 10 and 11. In dealing with these two types of resonance, transformations to fully isolate the "slow" evolution are needed. The conserved quantities in the two-dimensional systems that are the angular momenta conjugate to the "fast" angles in the four-dimensional systems are

$$H_{\Delta\omega} = \frac{e_\mathrm{P}^2 + i_\mathrm{P}^2}{2} \tag{21}$$

for the resonance in $\Delta\omega$ and

$$H_{\Delta(\Omega+\varpi)} = \frac{e_\mathrm{P}^2 - i_\mathrm{P}^2}{2} \tag{22}$$

for the resonance in $\Delta(\Omega + \varpi)$, respectively.

Similar to the concept resonance width, we use the amplitude of the oscillation of inclination near the separatrix between libration and circulation as an indicator of the strength of the resonance. It is then observed that, the resonance in $\Delta\Omega$ is the strongest, which may be the reason why it was the first to be identified (Christou 2005). In Fig. 8, we observe that the amplitude of the variation of inclination in $\Delta\Omega$ resonance can be as high as ≈ 0.005. The strengths of the resonances in $\Delta\omega$ and $\Delta(\Omega + \varpi)$ are similar to each other: the amplitudes of the oscillation of inclination are $\lesssim 0.001$.

Since there is apparently no libration in $\Delta\varpi$ in the semianalytical model, the structure of the phase space for the circulation should be trivial. Hence, we omit its phase diagram. Similar with the reasoning above, in the case where the slow angle is $\Delta\varpi$, the conserved quantity is i_P.

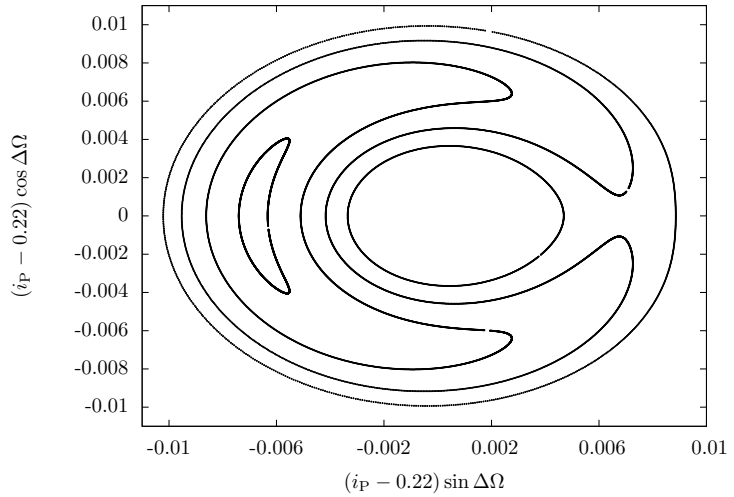

Fig. 8 Phase diagram for the nodal resonance in $\Delta\Omega$. All the orbits in this diagram share the same semimajor axis and the same conserved eccentricity, which are those of Lysithea. We subtract 0.22 from i_P mainly to highlight the topological structure; the value of 0.22 has been empirically chosen. Cf. Fig. 3

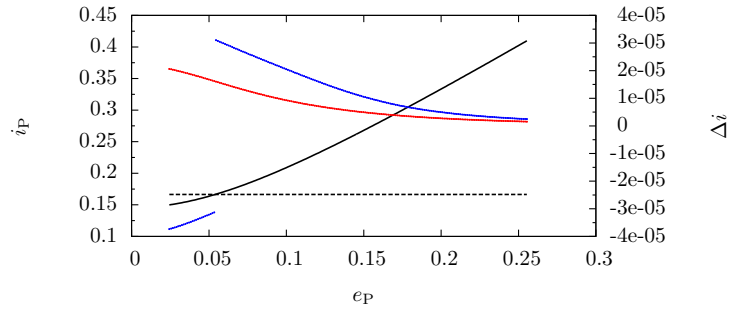

Fig. 9 The relative positions of the two equilibrium points of the nodal resonance. Left y-axis: the intersection of the SEPR in Ω with the $a = a_P$ plane (black solid curve) and the inclination of Himalia (horizontal dashed line); right y-axis: distance from the equilibrium point with $\Delta\Omega = \pi$ (the stable one) to the black curve in terms of inclination (red) and distance from the equilibrium point with $\Delta\Omega = 0$ (the unstable one, blue); x-axis: the varying eccentricity as a parameter

4 N-body simulations

Mainly due to the expansion in inclination, the semianalytical approach above is formally not accurate for the real Himalia group although it does serve to illustrate the dynamics. We also need to confirm whether these resonances identified by our semianalytical model

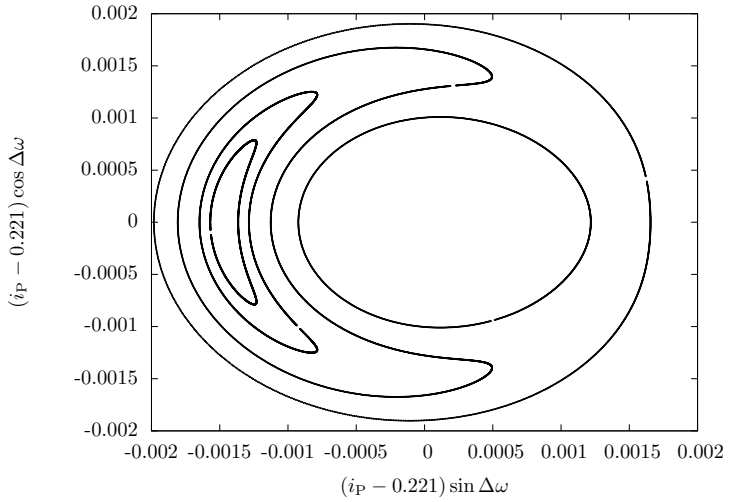

Fig. 10 Phase diagram for the resonance in $\Delta\omega = \Delta(\varpi - \Omega)$. Trajectories in this figure have the same semimajor axes and the same conserved quantity $H_{\Delta\omega} = (e_P^2 + i_P^2)/2$. Intuitively, for any give $H_{\Delta\omega}$, we can solve for e_P and i_P so that, $d\Delta\omega/dt = 0$ and this is a point on the corresponding SEPR in ω. However, the solution sometimes does not exist, which is the exact case for the $H_{\Delta\omega}$ prescribed by the elements of Lysithea. Thus we choose the point in the SEPR with the same semimajor axis and eccentricity as Lysithea. Then we use the $H_{\Delta\omega}$ of this point for all the trajectories plotted here. Cf. Fig. 5

survive in the full problem. For these reasons we perform extensive N-body simulations[6] to explore the parameter space of the real satellites.

The most important questions we wish to answer here are (i) how well the properties of these resonances are represented by the semianalytical model and, (ii) the possibility for a fictitious member of the family to be involved in such resonances. To explore these, an ensemble of massless test particles are integrated with Jupiter, the Sun and Himalia.

Beaugé and Nesvorný (2007) used the metric

$$d^2 = C_a(\Delta a/a)^2 + C_e(\Delta e)^2 + C_i(\Delta \sin i)^2 \tag{23}$$

to represent the distance from a satellite to the centre of a family in the proper element space (C_a, C_e and C_i are constant for a specific irregular satellite family). They proposed that for the Himalia family, a satellite with $d \lesssim 320$ m/s could be regarded as a member[7]. If generating test particles with the above criterion only, we produce an ensemble of particles with the eccentricity in the range $(0.03, 0.3)$ and inclination between $(23^\circ, 33^\circ)$. These are too large, considering that the corresponding ranges for the real family are about $(0.11, 0.22)$ and $(27^\circ, 29^\circ)$. To represent better the real family and to enhance the number density of particles in (a, e, i) space, we further require the eccentricity to be less than 0.1 and the

[6] All N-body simulations are implemented with the general Bulirsch-Stoer algorithm in the MERCURY package (Chambers 1999; Hahn and Malhotra 2005) with a tolerance 10^{-12}. Over an integration time of 10^8 yr, the errors in energy and angular momentum are both of order 10^{-10}.

[7] Note that, when they published the paper, four satellites: Himalia, Elara, Leda and Lysithea were confirmed as group members. The recently recovered fifth member, Dia, has the largest semimajor axis and eccentricity. Our simple experiments show that the criterion has to be updated to $d \lesssim 510$ m/s to include Dia. In this paper, we stick to the results of Beaugé and Nesvorný (2007).

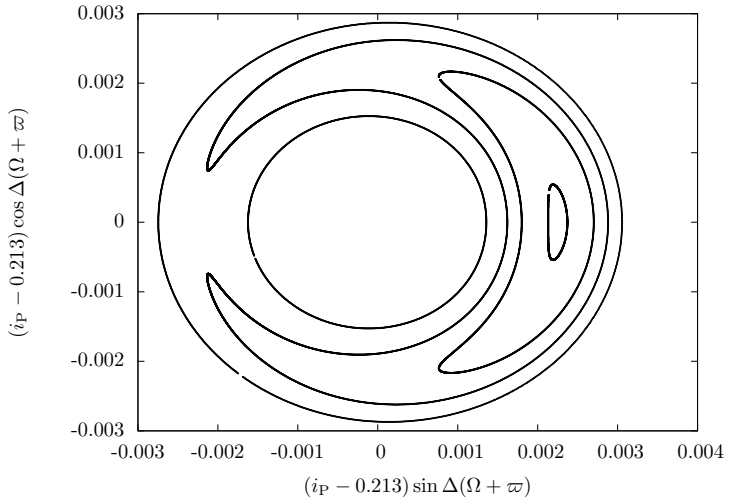

Fig. 11 Phase diagram for the resonance in $\Delta(\Omega+\varpi)$. Again, the curves possess the same semimajor axes and the same conserved quantity $H_{\Delta(\Omega+\varpi)} = (e_P^2 - i_P^2)/2$ that is chosen in a similar procedure as in Fig. 10. Cf. Fig. 6

inclination less than 2° from the family mean values; these two values are approximately twice those of the actual family. We do not apply specific restrictions on the semimajor axes as long as they fulfil the distance criterion. The final distribution of the test particles is: $a \in (0.745\text{AU}, 0.795\text{AU})$, $e \in (0.06, 0.26)$ and $i \in (26^\circ, 30^\circ)$. We generate 1000 such particles. Strictly speaking, the metric is valid for proper elements. We have applied it to osculating elements for simplicity. The particles, along with Jupiter, Sun and Himalia[8], are integrated for 100 Myr (about 5.3×10^7 in our time unit). Our integrations take place in a jovi-centric reference system. Following Hinse et al. (2010), we have changed the longitudes of pericentre by adding a π so that, the elements are correct in the jovi-centric frame. The solar eccentricity $e_\odot$ has been set to zero.

Our N-body runs confirm the existence of the resonances in $\Delta\Omega$, $\Delta\omega$ and $\Delta(\Omega+\varpi)$ and discover another one involving the angle $\Delta\varpi$. We present examples of them in the following subsection. In Subsect. 4.2, a statistical study of the resonances to address question (ii) stated in the beginning of this section is presented.

4.1 Resonances in N-body simulations

In Fig. 12, we show a typical example of a test particle in (temporary) nodal libration with Himalia. As in Christou (2005), the quantities e, i are averaged in a $\sim 5 \times 10^4$ time window to suppress the short-period oscllations. Some of these fluctuations come from the Kozai cycle.

The N-body simulations agree well with the semianalytical model in reproducing the general features of the nodal resonance, e.g., the centre and period of libration in $\Delta\Omega =$

[8] In the N-body simulations, the initial osculating elements of the real objects are taken from the JPL HORIZONS System http://ssd.jpl.nasa.gov/?horizons.

$\Omega_P - \Omega_H$ (π and 10^6 respectively), the corresponding oscillation in inclination and the failure of the resonance to excite the eccentricity. Inspecting the example in Fig. 12 in detail, it is found that, when the signed distance to the SEPR in (a,e,i) space, measured in Δi (top panel, the solid curve), is around the peak, $\Delta\Omega$ increases and when Δi is near the trough, $\Delta\Omega$ decreases. This is consistent with the semianalytical example (Fig. 3) in the sense that when the particle moves above the SEPR with higher inclination, it has higher nodal precession rate than Himalia (while its absolute value is lower since the rate is negative), and vice versa; as $\Delta\Omega$ approaches zero, the particle is pushed to cross the surface, causing the libration. However, in this example, the distance does not oscillate exactly around zero, but slightly below it. We suggest, this is because of the simplifications we made in Sect. 3.3 in constructing the semianalytical model and especially, in calculating the SEPR; in the full problem, such oscillations should be about zero. Alternatively, if we use the fit to the data from the N-body simulations (see Subsect. 4.2 and particularly, Eq. (27) and Fig. 19), the result turns out to be better. When in libration, the distance Δi (the dashed curve in the top panel) does oscillate around zero. Also apparent is that, before about 1.4×10^7, the distance remains smaller than zero and $\Delta\Omega$ keeps decreasing; then from roughly 1.9×10^7, the angle, after passage through libration, becomes increasing, with the distance above zero.

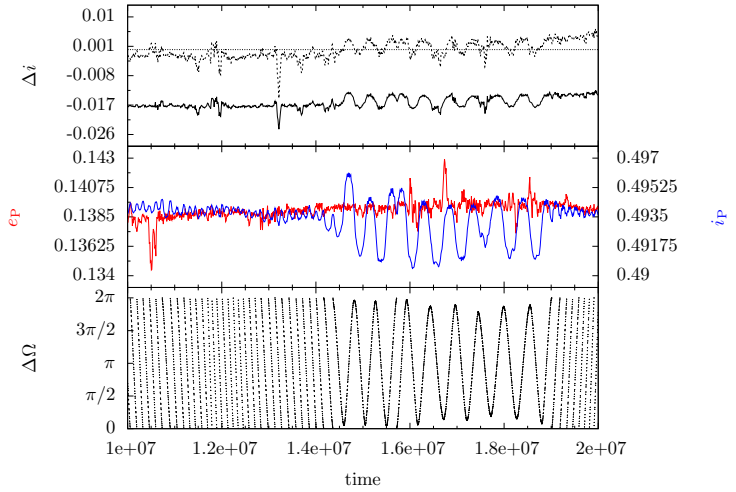

Fig. 12 An example of the libration in $\Delta\Omega = \Omega_P - \Omega_H$ from the N-body simulations. Cf. Figs. 3 and 8. Top panel: distance Δi measured as Δi to the SEPR; middle panel: e (red) and i (blue); bottom panel: $\Delta\Omega$; x-axis: time in our adopted unit. It is evident that, when in libration, i (but not e) is modulated on a timescale of 10^6. The distance Δi has the same meaning as in Fig. 3: the solid curve is the distance to the SEPR from semianalytical model (11); the dashed one is related to the fitted surface (Cf. Eq. (27) and Fig. 19); the horizontal dotted line marks a value of zero for Δi

In Fig. 13 we show an example of the resonance in $\Delta\omega = \Delta(\varpi - \Omega) = \omega_P - \omega_H$. As observed by our integrations of the semianalytical model (Fig. 5), the angle $\Delta\omega$ librates around π. The variation of the eccentricity and inclination is anti-correlated. This is reminiscent of the Kozai cycle.

We show an example for the resonance in $\Delta(\Omega + \varpi) = (\Omega_P + \varpi_P) - (\Omega_H + \varpi_H)$ as the lower panels in Fig. 14. This test particle evolves from circulation into libration, leaves

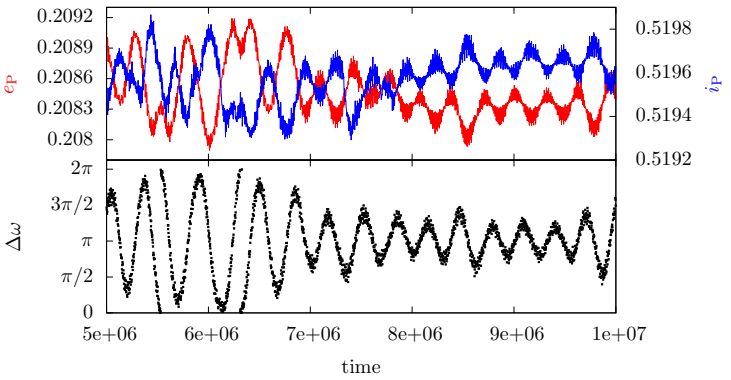

Fig. 13 An example of the libration in $\Delta\omega = \omega_P - \omega_H$. Cf. Figs. 5 and 10. Top panel: e (red) and i (blue); bottom panel: $\Delta\omega$; x-axis: time

libration and enters libration again. Here, the evolution of eccentricity and inclination is correlated: maxima (or minima) of e and i occur at the same time. Interestingly, for this particular example, the rate of circulation of the angle $\Delta\omega$ is not much faster than that of $\Delta(\Omega+\varpi)$. In the upper two panels, we show an enlargement of each of the lower two panels of Fig. 14. The short-period and anti-correlated evolution of eccentricity and inclination appear superposed on the long-period correlated evolution. We believe that such short-period effects are related to the circulation of $\Delta\omega$. Since the resonances are so close together in (a,e,i) space (see Figs. 4 and 19), it is not surprising such slow circulation of an angle exists inside the libration region of another angle.

Apart from the three types of resonance that appear in the semianalytical model and confirmed by our N-body runs here, we observe another type involving the angle $\Delta\varpi = \varpi_P - \varpi_H$. We illustrate it with an example in Fig. 15. The resonance in this angle seems to be the weakest as the resonant angle and action do not behave as regular as those in other three resonances. For the resonance in $\Delta\varpi$, we expect that, while the inclination remains nearly constant on the long term, the eccentricity oscillates periodically in accordance with the libration in $\Delta\varpi$. However, the resonance appears to be highly unstable in the sense that, (i) the libration in $\Delta\varpi$ is intermittent and that (ii) the oscillation of eccentricity does not correlate well with the variation of the angle. In Sect. 5, we will further explain this. The libration in $\Delta\varpi$ will be referred to as "apsidal libration" or "apsidal resonance" thereafter.

4.2 Statistics of the N-body simulations

Using the high number of libration episodes observed in our simulations, we can draw some statistical conclusions.

Out of the 1000 test particles, 37 are found to be in nodal resonance for longer than about 10^6 (by visual inspection); among those 37, 32 show libration for time spans $\gtrsim 3\times10^6$. A duration of 10^6 corresponds to approximately two cycles of the nodal libration.

To identify episodes of libration automatically in the time series, we implement two different approaches. The first approach uses the discrete Fast Fourier Transform (FFT) algorithm in the package "Fastest Fourier Transform in the West" (Frigo and Johnson 2005) to extract the periods and amplitudes of the periodic terms in the time series for $\Delta\Omega$ and i;

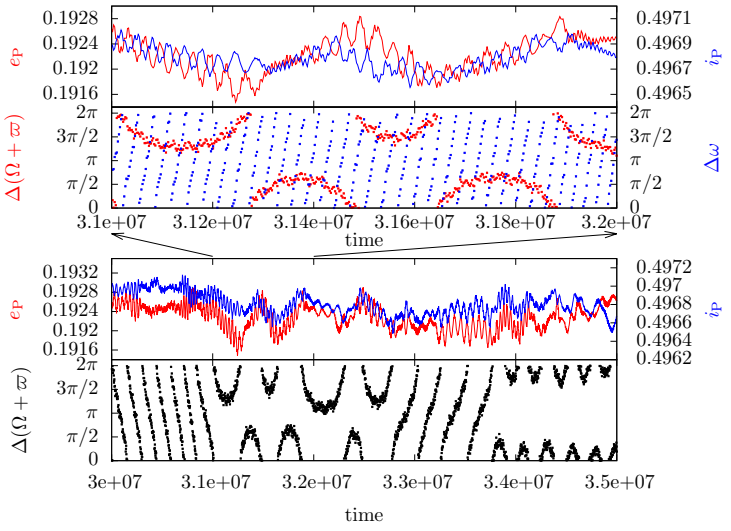

Fig. 14 An example of the libration in $\Delta(\Omega+\varpi) = (\Omega_P+\varpi_P) - (\Omega_H+\varpi_H)$ from the N-body simulations. Cf. Figs. 6 and 11. In the lower two panels: top panel: e (red) and i (blue); bottom panel: $\Delta(\Omega+\varpi)$; x-axis: time. The two upper panels represent enlargements of each of the bottom two panels: top panel: e (red) and i (blue); bottom panel: $\Delta(\Omega+\varpi)$ (red) and $\Delta\omega$ (blue); x-axis: time

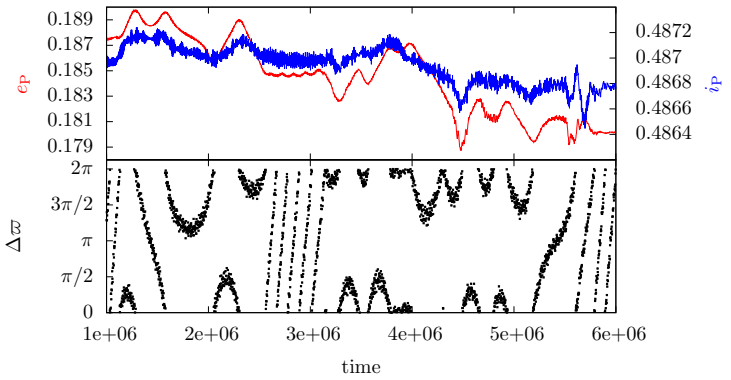

Fig. 15 An example of the libration in $\Delta\varpi = \varpi_P - \varpi_H$. Cf. Fig. 7. Top panel: e (red) and i (blue); bottom panel: $\Delta\varpi$; x-axis: time

then we identify and compare the dominant periods of the two. In the Fourier spectrum, the distribution of power as a function of period around the peak satisfies the normal distribution

$$P(x) = A\, e^{-\frac{(x-\mu_0)^2}{2\sigma_0^2}}, \tag{24}$$

where $P(x)$ is the strength at period x, A a scaling factor, μ_0 the centre of the normal distribution and σ_0 its dispersion. Taking the logarithm of both sides, we have

$$\log P(x) = \log A - \frac{(x-\mu_0)^2}{2\sigma_0^2}. \tag{25}$$

We fit this quadratic function to the data to extract the strongest period μ_0 and its strength $P(\mu_0)$. We have tried Gaussian fitting of the defined original strength and it often does not converge. To improve the procedure, we instead weigh our data in an iterative process. The weight is designed so that, points with periods closer to μ_0 and/or with larger strength P are more important; the weight function is

$$W_n = \frac{1+(P_n/\bar{P})^M}{1+|x_n-\mu_0|/\Delta x}, \tag{26}$$

in which (x_n, P_n) is a (period, strength) combination from the FFT analysis, W_n its weight, $\bar{P}$ the mean strength of all periods, Δx the total coverage in period and M a free parameter that controls the importance of the periods with different strength P. The value of μ_0 is updated after each iteration. This process continues until either μ_0 and $P(\mu_0)$ converge or do not. The analysis of inclination is complicated as it often shows multiple local extrema. Thus for inclination, if M is too large, μ_0 and $P(\mu_0)$ can converge towards a local extremum. For $\Delta\Omega$, the fluctuation is smaller, and a larger M allows us to achieve a better estimate of the strongest period. From experiments, we choose $M = 20$ for $\Delta\Omega$ and 4 for i; we use (x_n, P_n) only when $x_n \in (3\times10^5, 9\times10^5)$ to reduce the influences of irrelevant periods. In addition, we apply the criterion that if the fitted $P(\mu_0)$ is too small, we do not recognise the peak as real. In this way, we can identify all the 32 resonant particles with total time in libration $\geq 3\times10^6$, without any false positives.

Shown in Fig. 16 is the FFT analysis and the fitting results of the same test particle as in Fig. 12. Out of the entire integration time of 5.3×10^7, the total duration in libration is roughly 7×10^6. This is $(7\times10^6)/(5.3\times10^7) \approx 0.13$ of the entire integration and it generates a strong enough signature in FFT analysis that enables us to detect the libration. The period of nodal libration from the fit is 5.31×10^5 for this particle whereas the average period of the 32 cases is 5.73×10^5. As stated above, the determination of libration period in terms of $\Delta\Omega$ is more reliable owing to the higher value of M in the weight function (26); the two periods are from the analysis of $\Delta\Omega$.

However, the method described above does not work well for the resonances in $\Delta\omega$, $\Delta(\Omega+\varpi)$ and $\Delta\varpi$. We suggest this issue mainly results from the different behaviour of the resonances. For instance, in Fig. 14 for the resonance involving $\Delta(\Omega+\varpi)$, we see that the behaviour in the time range $(3.1\times10^7, 3.25\times10^7)$ and in $(3.36\times10^7, 3.5\times10^7)$ are visually different. Indeed, in the former, the particle is closer to the separatrix with larger amplitude and longer period compared to the latter one where the particle is near the libration centre. In nodal libration, the librator tends to stay near the separatrix (see Fig. 12); this may help to generate strong FFT signals[9]. Also these resonances are weaker with smaller amplitudes in the oscillations of e and/or i compared to the nodal resonance. These two factors may cause the failure of the above method to identify these episodes of libration for the three resonances.

To provide a universal approach valid for all the resonances, we introduce the following method which detects libration depending on the behaviour of the angles only.

[9] The particle in Fig. 18 described below is not a typical example: for a librator to be stable for 5.3×10^7, it has to lie well within the resonance. Most librators only pass through libration.

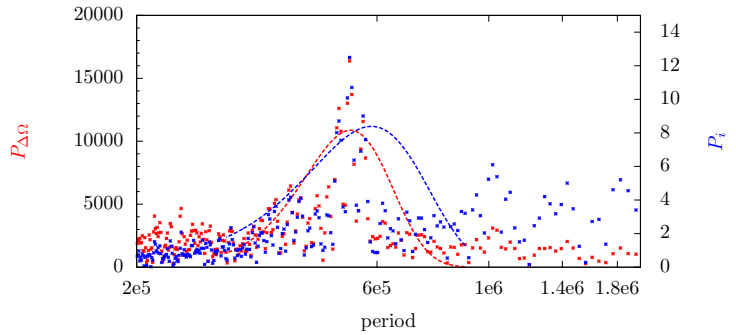

Fig. 16 The FFT analysis results and the represented fit in period-strength coordinates for $\Delta\Omega$ and i. Left y-axis: the FFT algorithm generated strength (point, red) and fitted strength (dashed curve, red) for $\Delta\Omega$; right y-axis: the FFT algorithm generated strength (point, blue) and fitted strength (dashed curve, blue) for i; x-axis: period. This is the analysis of the same particle as in Fig. 12

The basic idea is that principally, when an angle is in libration, it cannot cross the point that is π away from the libration centre and it must cross the libration centre regularly. For instance, in the case of nodal libration (i.e., when the libration centre is π), the angle $\Delta\Omega$ should not cross 0 and it is supposed to cross π periodically. If this state of affairs persists, we recognise it as a libration event. Additionally, we require the frequency of crossing the libration centre and the rate of the librating angle to be within plausible ranges. Therefore, the addition of these filters reduces significantly the number of false positives. In testing the method for nodal libration, we empirically choose the parameters so that it retrieves all the 32 librators found by the FFT-based method and without false positives. In this respect, the two methods are mutually consistent.

With this method, we find 32, 29, 19 and 11 particles in resonances involving $\Delta\Omega$, $\Delta\omega$, $\Delta(\Omega+\varpi)$ and $\Delta\varpi$, respectively.

In the N-body simulations, the evolution of eccentricity and inclination often experiences irregular short-period variations. It is then difficult to estimate the strengths of the resonances in terms of the amplitudes of the actions. Instead, we use the term "stability" to describe the resonances in real N-body simulations. We define stability as the longest duration of a single libration event from within the set of all such events. We extract the time duration for each libration event of the four resonances; we plot the distribution of durations of all such events in Fig. 17. The nodal resonance is the most stable, as it can lock a test particle in libration for $\gg 10^7$. Actually, we even have two particles remaining in libration for the entire integration of $\approx 5.3\times10^7$; see Fig. 18. The resonances in $\Delta\omega$ and $\Delta(\Omega+\varpi)$ are similarly stable; both can stay in libration for up to $\approx 10^7$. The resonance in $\Delta\varpi$ is the least stable: the libration cannot survive longer than $\approx 5.6\times10^6$. These results correlate with the strength estimates in Subsect. 3.7: the resonance with the largest amplitude is the most stable.

We compute the mean orbital elements of a librator when inside resonance and plot them in Fig. 19. We only use the averaged elements inside the libration, since as noted by Christou (2005), the elements may experience sudden changes in entering and/or leaving libration (e.g., Figs. 14 and 21). In the same figure, we show the following quadratic fit for each type of the resonances:

$$i = A_0 + A_1 a + A_2 e + A_3 a^2 + A_4 ae + A_5 e^2 \tag{27}$$

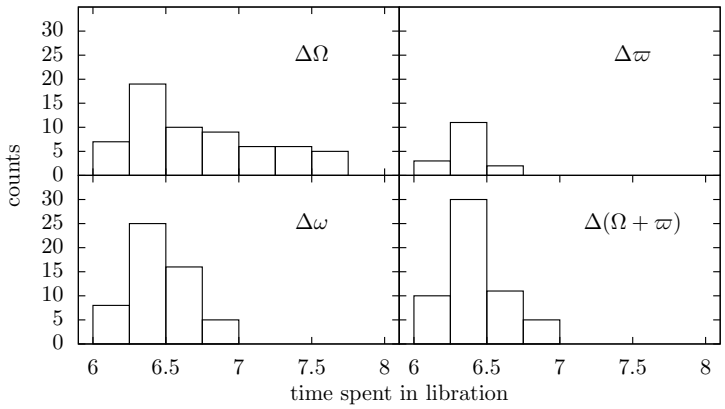

Fig. 17 The distribution of time spent in resonance of each libration event. Top-left: resonance involving $\Delta\Omega$; bottom-left: $\Delta\omega$; top-right: $\Delta\varpi$; bottom-right: $\Delta(\Omega+\varpi)$; *y*-axis: the numbers of libration events that spend the corresponding time in libration; *x*-axis: logarithmic time in the power of 10

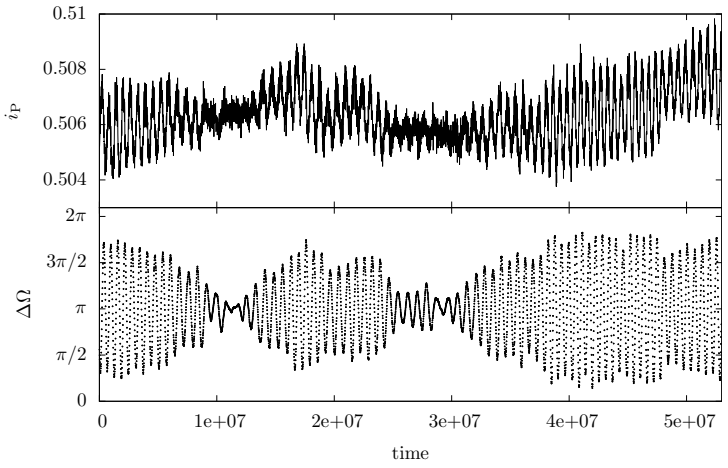

Fig. 18 A particle that stays in nodal libration for the entire integration duration of 5.3×10^7. Top panel: i; bottom panel: $\Delta\Omega$; *x*-axis: time

in which the A_j, $j=1,\ldots,5$, are the coefficients to be determined. These surfaces can be regarded as the SEPRs in the full problem since they originate from N-body simulations. Comparing them with the surfaces from semianalytical theory in Fig. 4, we find that the semianalytical model reproduces the relative positions and the overall slopes and shapes of the surfaces fairly well. The main reason for the differences between the two models for large inclination is that, the oscillation of eccentricity inside a Kozai cycle is not small here, contrary to our assumption of small variation of eccentricity in deriving Eq. (11). The fitted surface for Ω has been used to plot the distance to the SEPR in Fig. 12 (top panel, dashed curve). As a reference, the real family members are shown as well. As expected, Lysithea is close to the SEPR for Ω.

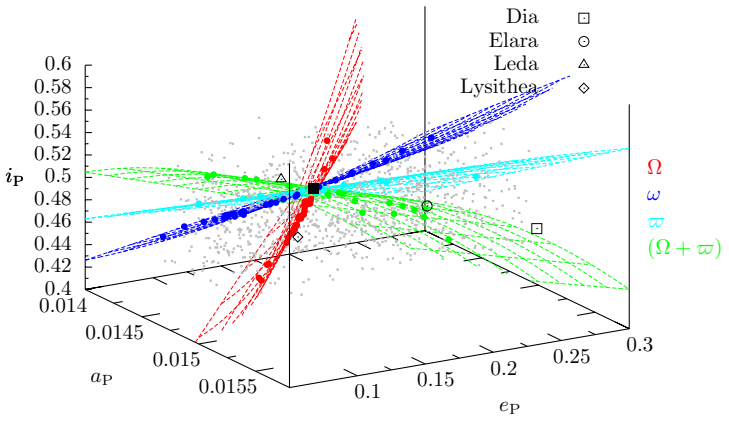

Fig. 19 The positions of the librators found in N-body simulations and the corresponding fitted SEPRs in (a,e,i) space in comparison with all integrated particles and with the real family members. The big round points with different colours represent the librators of the four types. The surfaces with corresponding colours are the fitted SEPRs. The small grey points are the 1000 test particles. The unfilled square, circle, triangle and diamond represent Dia, Elara, Leda and Lysithea, respectively. The black square is Himalia, again

To better highlight the positions of the resonant particles with respect to the SEPRs, we perform another set of simulations with 2×400 test particles. The generation of initial conditions is, by and large, the same as the previous simulations except that here the initial osculating semimajor axes only assume one of the two values $a_1=0.98$ and $a_2=1.02$ times the family mean semimajor axis. Then we plot the averaged e and i of the librators found in these 2×400 particles in the (e,i) plane and compare them with the positions of the curves of equal precession rate (the intersections of the SEPRs with the $a=a_1$ and $a=a_2$ planes) in Fig. 20. Again, the curves of equal precession rate from semianalytical model (solid curves) agree with those from the fit (dashed curves). Note that, although the initial osculating semimajor axes are uniquely defined, they can vary significantly over the course of the simulations; thus the mean a could be different from a_1 and a_2. This explains the excursion of a point from its corresponding fitted curve. For example, in the lower panel, the semimajor axis of the curves is exactly a_1 while for the points, the semimajor axes may be slightly different.

With the 1000 and 2×400 test particles, we have 54, 52, 38 and 28 in resonances of $\Delta\Omega$, $\Delta\omega$, $\Delta(\Omega+\varpi)$ and $\Delta\varpi$. They are all considered in fitting (27) while in Figs. 17 and 19, only the 1000 particle integration results are plotted. We have visually checked these code detected librators and confirm that they are actual librators. However, since our method is insensitive to short duration libration events, more short-lived librators are likely.

As noted in Christou (2005), it was possible that the nodal resonant passage had a net effect in the sense that the inclination, after the libration passage, could change $\sim0.1^\circ$, mostly increasing. In our simulations, we have confirmed the changes of similar amplitude; we find both directions are possible. Here, we show an example in Fig. 21. These resonance-induced changes and the cumulative long-term consequences will be addressed in a forthcoming paper.

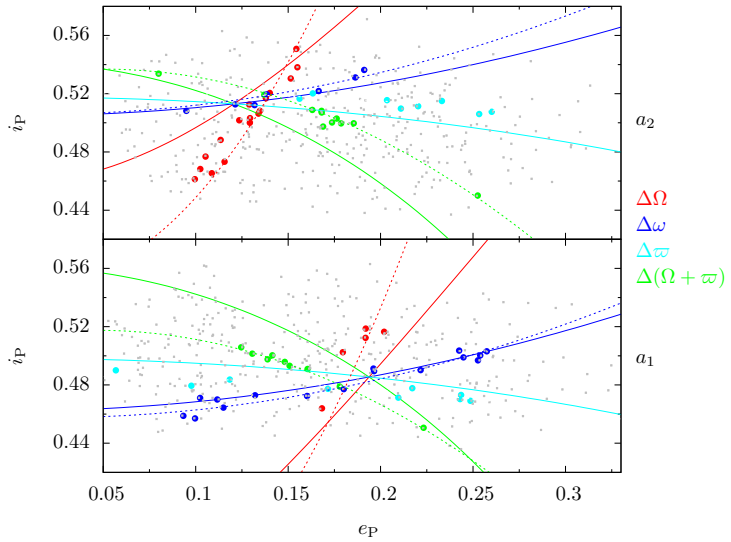

Fig. 20 The test particles that pass through the four types of resonance in the simulations with fixed initial as and the corresponding curves of equal precession rate. Top panel: results with $a_P = a_2$; bottom panel: results with $a_P = a_1$; y-axis: i; x-axis: e. Plotted here is the mean eccentricity and inclination of the librators (of the four resonances and for the time slots in libration) as coloured round points. The solid coloured curves are from Kozai potential (11) and the dashed curves are from the fit (27). Small grey points are all the 2×400 particles

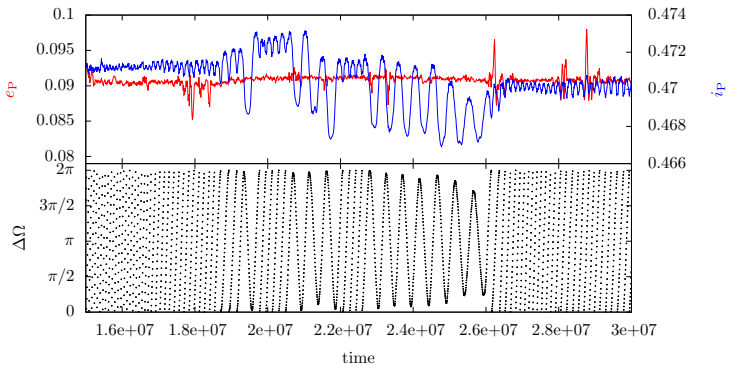

Fig. 21 An example of the change in inclination after passing through nodal resonance. This particular particle experiences a decrease of ~ 0.001 in inclination after the resonant passage

5 Conclusion and discussion

We have investigated the dynamics of the Himalia irregular satellite group in a restricted four-body problem scheme where Jupiter, Sun and the satellite Himalia have finite masses while the test particle, representing a fictitious group member, is massless. We combine the Kozai with coorbital theories to construct a unified semianalytical model; the "fast" effects (operating on timescales comparable to that of a Kozai cycle) are removed. Then we arrive

at a "slow" four-dimensional system. In this system, we are able to reproduce the main characteristics of a libration in $\Delta\Omega$ first observed in the numerical simulations in Christou (2005). We also identify two additional types of resonance involving the angles $\Delta\omega$ and $\Delta(\Omega+\varpi)$; their locations in phase space can be approximated by the surfaces of equal precession rate (SEPRs). In reducing the systems to two-dimensional ones, we determine the phase space structure for each of the three resonances. Using numerical integrations of the full Newtonian equations of motion, we confirm the results of the semianalytical model regarding the three types of resonance and find a fourth type involving $\Delta\varpi$. We analyse the occurrence rate and stability of these resonances in the N-body simulations. The libration periods of these four resonances are all of order 10^6; specifically, the FFT-based mean period of nodal resonance is 5.73×10^5 ($\sim$ 1.08 Myr). The main properties of the resonances are listed in Table 1.

Table 1 Summary of the properties of the four resonances studied in this work

libration angle	libration centre	conjugate action	conserved quantity	relation of $e_{\rm P}$ and $i_{\rm P}$	amplitude of $e_{\rm P}$ and/or $i_{\rm P}$	stability
$\Delta\Omega$	π	$i_{\rm P}$	$e_{\rm P}$	-	$\sim10^{-3}$	most stable
$\Delta\omega$	π	$e_{\rm P}, i_{\rm P}$	$(e_{\rm P}^2+i_{\rm P}^2)/2$	anti-correlated	$\sim10^{-4}$	moderately stable
$\Delta(\Omega+\varpi)$	0	$e_{\rm P}, i_{\rm P}$	$(e_{\rm P}^2-i_{\rm P}^2)/2$	correlated	$\sim10^{-4}$	moderately stable
$\Delta\varpi$	0	-	-	-	-	least stable

In the semianalytical approach, the "evection" terms (Yokoyama et al. 2008; see also Sect. 1) that relate the mean motion of the Sun with the apsidal rate of the satellite are omitted. The evection effect can be important for satellites far from the planet ($a\gtrsim r_{\rm H}/2$; $r_{\rm H}$ is the Hill radius of the planet) where the precession rate is fast. In the planar prograde case, the evection potential to the lowest order in α has the form (Frouard et al. 2010)

$$R_{\rm evec}\sim\frac{m_\odot\alpha^3}{a_\odot}e^2\cos(2\varpi-2\lambda_\odot), \tag{28}$$

where $\lambda_\odot$ is the Solar mean longitude. We have implemented the evection corrections as proposed in Cuk and Burns (2004) and found that it does not improve the precision of our model significantly. To be exact, with the corrections, we are still unable to approximate the nodal rate accurately enough to locate the position of the SEPR (in the full N-body model). Thus the evection correction is dropped. In addition, though the octupole solar perturbation potential is zero owing to the circular orbit assumed for the Sun (e.g., Krymolowski and Mazeh 1999), even higher order terms may contribute to the precession of the node and shift the location of resonance slightly. Regarding our simple way in removing ω in Eq. (4) and in reaching Eq. (11), there are semianalytical methods for this purpose (Henrard 1990). But that approach requires the introduction of new variables that have no apparent physical meaning, which we believe will complicate the interpretation of the results.

Our semianalytical model does not reproduce the apsidal resonance in $\Delta\varpi$. The original Kozai potential (4) is dependent on e only to order 2 but on i to higher orders (through $\cos i$) while in the coorbital potential (Eqs. (6) and (7)), e and i are symmetric. Thus this shortcoming of the semianalytical model results from the Kozai potential, specifically the truncated form of the solar forcing. The lack of higher order terms in e causes the absence

of $\bar{G}^2$ in the final Kozai potential (14) while $\bar{H}^2$ does exist. Thus after partial differentiation, the rate $\dot{\bar{g}}$ does not depend on its conjugate angular momentum $\bar{G}$ but $\dot{\bar{h}}$ does depend on $\bar{H}$. Hence we suggest that, the Kozai potential not only gives rise to the SEPRs, it must also play an important role in modulating $\dot{\bar{h}}$ (thus $\mathrm{d}\Delta\Omega/\mathrm{d}t$) through $\bar{H}$. Therefore, terms like $\bar{G}^2$ in the solar perturbation is needed for the apsidal libration, which is only possible in higher order terms in $\alpha = a/a_\odot$. Indeed, if we artificially add a term $\bar{G}^2$ in the Kozai potential, the resonance in $\Delta\varpi$ can be retrieved in the semianalytical model. We believe this is why we do not observe apsidal libration in the semianalytical model while it does appear in the N-body simulations. This is probably why the apsidal resonance is the most unstable and the weakest (see Figs. 15 and 17).

Although our semianalytical model is truncated in e and i, we test it with real Himalia group inclinations (≈ 0.5) and find that, the model does reproduce the three resonances at these inclinations. However, by dividing the real inclinations by a factor of 3, the e and i are similarly small and more consistent with the assumptions made in deriving the coorbital interaction potential (6) (Hénon and Petit 1986; Namouni 1999).

We have simplified the problem to a restricted four-body problem model. In reality, perturbations such as the oblateness of Jupiter and the effects of other planets exist. When these additional factors are considered, we suggest these resonances may still persist. In our analysis, the solar perturbation mainly arrests relative precession and makes the resonances possible, though terms like $\bar{H}^2$ do contribute directly to give rise to the resonances. On the timescales we are interested in, it has been simplified in the form (14) containing no angles. When a more elaborate model is constructed, probably similar simplifications can be made and small changes in the resonance locations (in the form of the SEPRs) will likely occur. In Christou (2005), Saturn and the jovian oblateness were taken into account and in such a configuration, he found the resonance in $\Delta\Omega$. Including other planets may introduce additional dynamical effects such as secular resonances (see, e.g., Beaugé and Nesvorný 2007; Frouard et al. 2011).

Similar to high order mean motion resonance (Moons 1997) and secular resonance (Bottke et al. 2001), resonances involving other combinations of $\Delta\Omega$ and $\Delta\varpi$ may exist. They may be weaker and less stable, compared to the resonances described in this paper.

As shown in Figs. 4 and 19, the SEPRs are close together to each other, especially near the massive satellite. Consequently, the resonances may interact with each other and give rise to chaos; e.g., Fig. 14. Considering that Himalia may give other group members random kicks during close encounters, it is not strange that a test particle may pass through more than one type of resonance if we extend the N-body simulations long enough. Actually, in our 100 Myr integration, we observe an example transiting from libration in $\Delta\varpi$ to libration in $\Delta(\Omega+\varpi)$.

Considering that the retrograde irregular satellite groups are more prevalent in the solar system and that, they often have a much more massive member, the resonances explored in this paper for prograde satellites may have their counterparts in the retrograde case. For example, the Ananke and Carme groups of Jupiter have inclinations around 150° and 165°, respectively. However, the most massive members in the two groups are only 0.004 and 0.02 of the mass of Himalia (m_H) and this is possibly too small to allow resonance phenomena to exist. As an experiment, we have run N-body simulations to test if a prograde massive satellite of $0.01m_\mathrm{H}$ can induce nodal resonance and the results is positive – such low masses may work. As the cases of evection phenomenon (described in Sect. 1), the definition of ϖ becomes the difference between Ω and ω for retrograde orbits; it is possible that the

structure of the retrograde resonances is different, for instance, the libration centre may change. For the masses and orbital elements mentioned here, see footnote 1.

Recently, Novaković et al. (2015) reported a nodal resonance similar to the one discussed here. Their resonance is due to Ceres and could be responsible for the inclination dispersion in the Hoffmeister asteroid family. In their case, the main perturbation comes from Jupiter and the mass ratio between Ceres and Jupiter is of order 10^{-7}; in our situation, the mass ratio $m_{\rm H}/m_{\odot}$ is 10^{-12}, arguably a more extreme case. Due to the similar nature of the two problems, we suggest that other types of resonance (e.g., the one involving $\Delta\omega$) may exist in the asteroid belt.

Finally, in Fig. 19 we see that, Dia, Elara and Leda are near the SEPR in $(\Omega+\varpi)$ while Lysithea is close to the surface in Ω. To check whether the real satellites could be affected by the resonances, we perform an additional integration using the orbits of the real moons for 1000 Myr. We find that, Leda does enter the resonance in $\Delta(\Omega+\varpi)$. Thus some members of the actual family may have been affected by these resonances. This will be addressed in a future paper.

Acknowledgements DL thanks Dr. Matjia Ćuk for correspondences on the evection phenomenon. We are grateful for the helpful comments from two anonymous referees, increasing the quality of the paper. The authors wish to acknowledge the SFI/HEA Irish Centre for High-End Computing (ICHEC) for the provision of computational facilities and support. Astronomical research at the Armagh Observatory is funded by the Northern Ireland Department of Culture, Arts and Leisure (DCAL). Fig. 1 is produced using LibreOffice Draw; all the other figures are generated with gnuplot.

Appendix A Derivation of the "averaged" Kozai Hamiltonian

We derive the Kozai Hamiltonian (11) from its original form (4) here. First, we substitute e and i in Eq. (4) in terms of the angular momenta G and H. Then we solve for G so $G=G(F,H,\omega,const.)$, where $const.$ refers to combinations of k, $m_{\odot}$, a and $a_{\odot}$. Note that in this expression, F, H and $const.$ are all constant and only ω and G are variable. Furthermore, it can be shown with this equation that the variation in eccentricity during a Kozai cycle, Δe^2 is a small quantity (e.g., for Himalia's nominal orbit, $\Delta e^2 \lesssim 0.03$). Therefore, we assume that the angular momentum $G\propto\sqrt{1-e^2}$ can be expressed as

$$G^2 = b_0 + b_1\cos 2\omega + \ldots, \tag{29}$$

where the coefficients $b_1 \ll b_0$. We can then express b_0 and b_1 as functions of F, H and $const.$ by comparing the above equation with $G=G(F,H,\omega,const.)$. Now, if we further omit the term $b_1\cos 2\omega$ we have

$$G^2 = b_0 = b_0(F,H,const.) \propto 1-\langle e\rangle^2. \tag{30}$$

Here, $\langle e\rangle$ is not the e in the original Hamiltonian (4) but the averaged e over a Kozai cycle. Meanwhile, we also have $H^2\propto(1-\langle e\rangle^2)\cos^2\langle i\rangle$ and $\langle i\rangle$ is the averaged i. Then we solve Eq. (30) for F. So now F is a function of H, $b_0=G^2$ and $const.$. After substituting $\langle e\rangle$ and $\langle i\rangle$ into it, we arrive at the "averaged" Kozai Hamiltonian (11). The new eccentricity and inclination are constant under the solar forcing; for simplicity, we still use the old notations e and i.

Appendix B The non-canonical property of coorbital potential

As stated in Subsect. 3.3, the coorbital potential (6) (and hence (17)) is not canonical in the variables used in Eq. (16). To prove this, we presume it is canonical and introduce the following canonical transformations. For the first transformation, we name the variables on the left side as "absolute Cartesian" variables.

$$\begin{aligned}
\bar{G}_{\mathrm{y,H}} &= \sqrt{2\bar{G}_{\mathrm{H}}}\sin\bar{g}_{\mathrm{H}}, \quad \bar{G}_{\mathrm{x,H}} = \sqrt{2\bar{G}_{\mathrm{H}}}\cos\bar{g}_{\mathrm{H}};\\
\bar{H}_{\mathrm{y,H}} &= \sqrt{2\bar{H}_{\mathrm{H}}}\sin\bar{h}_{\mathrm{H}}, \quad \bar{H}_{\mathrm{x,H}} = \sqrt{2\bar{H}_{\mathrm{H}}}\cos\bar{h}_{\mathrm{H}};\\
\bar{G}_{\mathrm{y,P}} &= \sqrt{2\bar{G}_{\mathrm{P}}}\sin\bar{g}_{\mathrm{P}}, \quad \bar{G}_{\mathrm{x,P}} = \sqrt{2\bar{G}_{\mathrm{P}}}\cos\bar{g}_{\mathrm{P}};\\
\bar{H}_{\mathrm{y,P}} &= \sqrt{2\bar{H}_{\mathrm{P}}}\sin\bar{h}_{\mathrm{P}}, \quad \bar{H}_{\mathrm{x,P}} = \sqrt{2\bar{H}_{\mathrm{P}}}\cos\bar{h}_{\mathrm{P}}.
\end{aligned} \tag{31}$$

On the right-hand sides of the above expressions, $(\bar{g},\bar{G})$ and $(\bar{h},\bar{H})$ are conjugate Poincaré variables with subscripts "H" and "P" referring to Himalia and a particle, respectively. Then another transformation is introduced. The variables on the left are referred to as "relative Cartesian" variables.

$$\begin{aligned}
\bar{G}_{\mathrm{y,t}} &= \bar{G}_{\mathrm{y,P}}/\sqrt{2}+\bar{G}_{\mathrm{y,H}}/\sqrt{2}, \quad \bar{G}_{\mathrm{x,t}} = \bar{G}_{\mathrm{x,P}}/\sqrt{2}+\bar{G}_{\mathrm{x,H}}/\sqrt{2};\\
\bar{H}_{\mathrm{y,t}} &= \bar{H}_{\mathrm{y,P}}/\sqrt{2}+\bar{H}_{\mathrm{y,H}}/\sqrt{2}, \quad \bar{H}_{\mathrm{x,t}} = \bar{H}_{\mathrm{x,P}}/\sqrt{2}+\bar{H}_{\mathrm{x,H}}/\sqrt{2};\\
\bar{G}_{\mathrm{y,r}} &= \bar{G}_{\mathrm{y,P}}/\sqrt{2}-\bar{G}_{\mathrm{y,H}}/\sqrt{2}, \quad \bar{G}_{\mathrm{x,r}} = \bar{G}_{\mathrm{x,P}}/\sqrt{2}-\bar{G}_{\mathrm{x,H}}/\sqrt{2};\\
\bar{H}_{\mathrm{y,r}} &= \bar{H}_{\mathrm{y,P}}/\sqrt{2}-\bar{H}_{\mathrm{y,H}}/\sqrt{2}, \quad \bar{H}_{\mathrm{x,r}} = \bar{H}_{\mathrm{x,P}}/\sqrt{2}-\bar{H}_{\mathrm{x,H}}/\sqrt{2}.
\end{aligned} \tag{32}$$

This relates the variables with subscript "r" to the variables used in the coorbital theory as given by Namouni (1999); see the paragraph containing Eqs. (6)-(9).

Now note that, since we assume the coorbital potential is canonical in the original Poincaré variables, it should preserve the Hamiltonian property in the variables above. However, since the coorbital potential contains only the relative elements, i.e., in the relative Cartesian variables, it only depends on the variables with subscript "r". Hence, if we consider the Jupiter-Himalia-particle system. The quantities with subscript "t" will be conserved. However, this is not possible. Taking $\bar{G}_{\mathrm{y,t}} = \bar{G}_{\mathrm{y,P}}/\sqrt{2}+\bar{G}_{\mathrm{y,H}}/\sqrt{2}$ for instance. Since the test particle is massless, it should have no influence on Himalia and thus the second term on the right hand side $\bar{G}_{\mathrm{y,H}}/\sqrt{2}$ is constant. From the above reasoning, we know that, $\bar{G}_{\mathrm{y,t}}$ should be conserved. This means that, the first term on the right hand side, $\bar{G}_{\mathrm{y,P}}/\sqrt{2} = \sqrt{\bar{G}_{\mathrm{P}}}\sin\bar{g}_{\mathrm{P}}$ will no change. Similarly, $\sqrt{\bar{G}_{\mathrm{P}}}\cos\bar{g}_{\mathrm{P}}$, $\sqrt{\bar{H}_{\mathrm{P}}}\sin\bar{h}_{\mathrm{P}}$ and $\sqrt{\bar{H}_{\mathrm{P}}}\cos\bar{h}_{\mathrm{P}}$ should all be constant. If so, the orbital elements of the particle are not evolving under the perturbation of Himalia. Of course this is not true – the coorbital potential is not a Hamiltonian in the variables used here.

However, the level-curve like structure in the phase diagrams Figs. 8, 10 and 11 of the three types of resonance suggests the existence of a conserved quantity (a Hamiltonian) for these two-dimensional systems. We have tried to construct one of the form of $F_{\mathrm{T}} = F_{\mathrm{S}} + A \times R_{\mathrm{S}}$ (see Eqs. (16) and (17)), where A is a constant depending on some non-changing parameters. For instance, for the case of nodal resonance, A could be a function of the masses, the semimajor axes and the eccentricities (but not a function of inclinations). However, the solution for A seems to be nonexistent (at least for the nodal resonance). Thus we argue that, the conserved quantity of the two-dimensional systems might be of more complicated forms.

References

Beaugé, C., Nesvorný, D.: Proper elements and secular resonances for irregular satellites. Astron. J. **133**, 2537–2558 (2007)

Beaugé, C., Nesvorný, D., Dones, L.: A high-order analytical model for the secular dynamics of irregular satellites. Astron. J. **131**, 2299–2313 (2006)

Bottke, W. F., Vokrouhlický, D., Broz, M., Nesvorný, D., Morbidelli, A.: Dynamical spreading of asteroid families by the Yarkovsky effect. Science **294**, 1693–1696 (2001)

Burns, J. A.: The evolution of satellite orbits. In: Burns, J. A., Matthews, M. S. (eds.) Satellites, pp. 117–158. The University of Arizona Press, Tucson (1986)

Carruba, V., Burns, J. A., Nicholson, P. D., Gladman, B. J.: On the inclination distribution of the jovian irregular satellites. Icarus **158**, 434–449 (2002)

Carruba, V., Burns, J. A., Bottke, W., Nesvorný, D.: Orbital evolution of the Gefion and Adeona asteroid families: close encounters with massive asteroids and the Yarkovsky effect. Icarus **162**, 308–327 (2003)

Chambers, J. E.: A hybrid symplectic integrator that permits close encounters between massive bodies. Mon. Not. R. Astron. Soc. **304**, 793–799 (1999)

Christou, A. A.: Gravitational scattering within the Himalia group of jovian prograde irregular satellites. Icarus **174**, 215–229 (2005)

Cuk, M., Burns, J. A.: On the secular behavior of irregular satellites. Astron. J. **128**, 2518–2541 (2004)

Emelyanov, N. V.: The mass of Himalia from the perturbations on other satellites. Astron. Astrophys. **438**, L33–L36 (2005)

Frigo, M. and Johnson, S. G.: The design and implementation of FFTW3. Proc. IEEE. **93** pp. 216–231 (2005)

Frouard, J., Fouchard, M., Vienne, A.: About the dynamics of the evection resonance. Astron. Astrophys. **515**, A54 (2010)

Frouard, J., Vienne, A., Fouchard, M.: The long-term dynamics of the Jovian irregular satellites. Astron. Astrophys. **532**, A44 (2011)

Goldreich P.: History of the lunar orbit. Rev. Geophys. **4**, 411–439 (1966)

Hahn, J. M., Malhotra, R.: Neptune's migration into a stirred-up Kuiper Belt: a detailed comparison of simulations to observations. Astron. J. **130**, 2392–2414 (2005)

Hénon, M., Petit, J. M. Series expansions for encounter-type solutions of Hill's problem. Celest. Mech. **38**, 67–100 (1986)

Henrard, J.: A semi-numerical perturbation method for separable hamiltonian systems. Celest. Mech. Dyn. Astron. **49**, 43–67 (1990)

Hinse, T. C., Christou, A. A., Alvarellos, J. L. A., Goździewski, K.: Application of the MEGNO technique to the dynamics of Jovian irregular satellites. Mon. Not. R. Astron. Soc. **404**, 837–857 (2010)

Innanen, K. A., Zheng, J. Q., Mikkola, S., Valtonen, M. J.: The Kozai mechanism and the stability of planetary orbits in binary star systems. Astron. J. **113**, 1915–1919 (1997)

Jewitt, D., Haghighipour, N.: Irregular satellites of the planets: products of capture in the early Solar system. Annu. Rev. of Astron. Astro. **45**, 261–295 (2007)

Kozai, Y.: Secular perturbations of asteroids with high inclination and eccentricity. Astron. J. **67**, 591–598 (1962)

Krymolowski, Y., Mazeh, T.: Studies of multiple stellar systems - II. Second-order averaged Hamiltonian to follow long-term orbital modulations of hierarchical triple systems. Mon. Not. R. Astron. Soc. **304**, 720–732 (1999)

Lidov, M.: The evolution of orbits of artificial satellites of planets under the action of gravitational perturbations of external bodies. Planet. Space Sci. **9**, 719–759 (1962)

Lidov, M. L., Ziglin, S. L.: Non-restricted double-averaged three body problem in Hill's case. Celest. Mech. **13**, 471–489 (1976)

Luciani, J. F., Namouni, F., Pellat, R.: The kinetics of systems of planetesimals. Astrophys. J. **439**, 800–813 (1995)

Message, P. J.: The dominant features of the long period librations of the trojan minor planets. In: Rosser, J. B. eds. Space Mathematics, Part 2-Lectures in Applied Mathematics, Vol. 6, pp. 70–78. AMS, Providence, Rhode Island (1966)

Moons, M.: Review of the dynamics in the Kirkwood gaps. Celest. Mech. Dyn. Astron. **65**, 175–204 (1997)

Morais, M. H. M.: A secular theory for Trojan-type motion. Astron. Astrophys. **326**, 318–326 (1999)

Murray, C. D., Dermott, S. F.: Solar System Dynamics. Cambridge University Press, Cambridge (1999)

Namouni, F.: Secular interactions of coorbiting objects. Icarus **314**, 293–314 (1999)

Naoz, S., Farr, W. M., Lithwick, Y., Rasio, F. A., Teyssandier, J.: Secular dynamics in hierarchical three-body systems. Mon. Not. R. Astron. Soc. **431**, 2155–2171(2013)

Nesvorný, D., Alvarellos, J. L. A., Dones, L., Levison, H. F.: Orbital and collisional evolution of the irregular satellites. Astron. J. **126**, 398–429 (2003)

Nicholson, P. D., Ćuk, M., Sheppard, S. S., Nesvorný, D., Johnson, T. V..: Irregular satellites of the giant planets. In: Barucci, M. A., Boehnhardt, H., Cruikshank, D. P., Morbidelli, A., Dotson, R. (eds.) The Solar System Beyond Neptune, pp. 411–424. University of Arizona Press, Tucson (2008)

Novaković, B., Maurel, C., Tsirvoulis, G., Knežević, Z.: Asteroid secular dynamics: Ceres? fingerprint identified. Astrophys. J. **807**, L5 (2015)

Roy, A. E.: Orbital Motion. Adam Hilger, Ltd., Bristol. (1978)

Sheppard, S. S., Jewitt, D. C.: An abundant population of small irregular satellites around Jupiter. Nature **423**, 261–263 (2003)

Weisstein, E. W.: Polylogarithm. MathWorld–A Wolfram Web Resource. http://mathworld.wolfram.com/Polylogarithm.html (1995). Accessed 24 October 2015

Williams, J. G., Faulkner, J.: The positions of secular resonance surfaces. Icarus **46**, 390–399 (1981)

Yokoyama, T., Vieira Neto, E., Winter, O. C., Sanchez, D. M., Brasil, P. I. D. O.: On the evection resonance and its connection to the stability of outer satellites. Math. Probl. Eng. **2008**, 1–16 (2008)